The critical effects of matrices on cultured carcinoma cells: Human tumor-derived matrix promotes cell invasive properties

Wafa Wahbi, Erika Naakka, Katja Tuomainen, Ilida Suleymanova, Annamari Arpalahti, Ilkka Miinalainen, Juho Vaananen, Reidar Grenman, Outi Monni, Ahmed Al-Samadi, Tuula Salo

PII: S0014-4827(20)30084-7

DOI: https://doi.org/10.1016/j.yexcr.2020.111885

Reference: YEXCR 111885

To appear in: *Experimental Cell Research*

Received Date: 20 November 2019

Revised Date: 15 January 2020

Accepted Date: 31 January 2020

Please cite this article as: W. Wahbi, E. Naakka, K. Tuomainen, I. Suleymanova, A. Arpalahti, I. Miinalainen, J. Vaananen, R. Grenman, O. Monni, A. Al-Samadi, T. Salo, The critical effects of matrices on cultured carcinoma cells: Human tumor-derived matrix promotes cell invasive properties, *Experimental Cell Research* (2020), doi: https://doi.org/10.1016/j.yexcr.2020.111885.

The critical effects of matrices on cultured carcinoma cells: human tumor-derived matrix promotes cell invasive properties

Wafa Wahbi[1,2], Erika Naakka[1,2#], Katja Tuomainen[1,2#], Ilida Suleymanova[1,2], Annamari Arpalahti[1,2], Ilkka Miinalainen[3], Juho Vaananen[4], Reidar Grenman[5], Outi Monni[4], Ahmed Al-Samadi[1,2*&], Tuula Salo[1,2,6,7,8&]

1 Department of Oral and Maxillofacial Diseases, Clinicum, Faculty of Medicine, University of Helsinki, Helsinki, Finland

2 Translational Immunology Program, Faculty of Medicine, University of Helsinki

3 Biocenter Oulu Electron Microscopy Core Facility, University of Oulu, Oulu, Finland.

4 Applied Tumor Genomics Research Program, Faculty of Medicine, University of Helsinki, Helsinki, Finland 5 Department of Otolaryngology, Turku University, Turku, Finland.

6 Cancer and Translational Medicine Research Unit, University of Oulu, Oulu, Finland

7 Medical Research Centre, Oulu University Hospital, Oulu, Finland

8 Helsinki University Hospital, Helsinki, Finland

# Designates an equal contribution to this work.

& Supervised the work equally.

* Corresponding author: Ahmed Al-Samadi, Department of Oral and Maxillofacial Diseases, Clinicum, Biomedicum Helsinki 1, C223b P.O. Box 63 (Haartmaninkatu 8), 00014 University of Helsinki, Helsinki, Finland; E-mail: ahmed.al-samadi@helsinki.fi ; Tel: +358458947224.

Declaration of interests: The authors declare that they have no conflict of interest.

Abstract

The interaction between squamous cell carcinoma (SCC) cells and the tumor microenvironment (TME) plays a major role in cancer progression. Therefore, understanding the TME is essential for the development of cancer therapies.

We used four (primary and metastatic) head and neck (HN) SCC cell lines and cultured them on top of or within 5 matrices (mouse sarcoma-derived Matrigel®, rat collagen, human leiomyoma-derived Myogel, human fibronectin and human fibrin). We performed several assays to study the effects of these matrices on the HNSCC behavior, such as proliferation, migration, and invasion, as well as cell morphology, and molecular gene profile.

Carcinoma cells exhibited different growth patterns depending on the matrix. While fibrin enhanced the proliferation of all the cell lines, collagen did not. The effects of the matrices on cancer cell migration were cell line dependent. Carcinoma cells in Myogel-collagen invaded faster in scratch wound invasion assay. On the other hand, in the spheroid invasion assay, three out of four cell lines invaded faster in Myogel-fibrin. These matrices significantly affected hundreds of genes and a number of pathways, but the effects were cell line dependent.

The matrix type played a major role in HNSCC cell phenotype. The effects of the ECMs were either constant, or cell line dependent. Based on these results, we suggest to select the most suitable matrix, which provides the closest condition to the *in vivo* TME, in order to get reliable results in *in vitro* experiments.

Keywords: Cancer, Extracellular Matrix, Invasion, Migration, Tumor Microenvironment.

Introduction

Squamous cell carcinoma cells are notably affected by their microenvironment that mainly includes extracellular matrix (ECM) and tumor stromal cells, such as cancer-associated fibroblasts (CAF), immune and endothelial cells (1). ECM is a major component of the TME and it is composed of a variety of proteins, proteoglycans, and polysaccharides (2). The structure and physical properties of tumor-associated ECM differ from normal tissue stroma (3). Changes in the ECM properties may cause variation in collagen deposition, promote the ECM stiffness, and upgrade cell survival and proliferation (4,5). ECM could also affect tumor stroma cells, such as CAFs, immune and endothelial cells (6). Therefore, understanding the SCC microenvironment is essential for the development of cancer therapies, which targets not only the cancer cells but also their environment that allows them to proliferate and spread.

In vitro, cancer cells are generally studied in 2D plastic wells. This usually leads to a loss of several important elements, which could affect the cell behavior and phenotype, making the 2D system not representative of the *in vivo* situation. In order to provide a more physiological environment for the cells, culture systems using different ECM mimicking three-dimensional matrices were introduced. Even though several matrices, which are extracted from different species such as mouse, rat, bovine, or prepared from non-animal material (7), were proposed to be used in 3D cell culture assays, selecting the most appropriate matrix for each cell type is not straightforward.

In spite of presence of several matrices from different origins, a human tumour-derived matrix is still missing from the market. Our group has invented the first tumour-derived matrix “Myogel” which is derived from leiomyoma tissue (8). Myogel has been used in several cancer *in vitro* studies (1,9-12). Myogel proteome differs greatly from the commonly used mouse sarcoma–derived Matrigel (8). We have shown recently that Myogel enhance the proliferation of freshly isolated cancer cells from primary tumor compared to plastic and Matrigel (10). Additionally, based on our recent publication, Myogel also improved the predictability of head and neck cancer drug testing (12). This setup, applying Myogel coated wells in drug testing, could reduce the number of failure clinical trials and reduce the cost of the anti-cancer drug development.

Here, we aimed to investigate the effects of several human- and animal-extracted ECMs, on the head and neck (HN) SCC cells. We used mouse tumor-derived Matrigel®, rat tail collagen, human plasma fibronectin, human-derived fibrin, and human tumor-derived Myogel; Bovine serum albumin (BSA) and uncoated wells were used as negative controls. We selected four HNSCC cell

lines as a model of SCC cells: UT-SCC-24 (tongue) and UT-SCC-42 (larynx), including primary (A) and corresponding metastasis (B). We compared the effects of these matrices with the non-coated plastic analyzing cell morphology, proliferation, migration, and invasion. We also studied the effects of these matrices on the molecular profile of these cells using transcriptome profiling.

Materials and Methods

Cell lines

UT-SCC cell line series, UT-SCC-24A (Primary tongue cancer, RRID:CVCL_7826), UT-SCC-24B (Metastatic tongue cancer, RRID:CVCL_7827) and UT-SCC-42 (larynx), including primary (A, RRID:CVCL_7847) and metastatic (B, RRID:CVCL_7848). Were kindly provided by Prof. Grenman (Department of Otolaryngology, Turku University, Turku, Finland). UT-SCC cells were grown in DMEM-F12 medium (Gibco™/Invitrogen, Tokyo, Japan) supplemented with 10% foetal bovine serum, 1% penicillin/streptomycin and 250µg/mL amphotericin B (all from Sigma-Aldrich, St. Louis, Mo, USA). All the cell lines were cultured in a humidified incubator (37°C, 5% CO2, 95% humidity, Binder, Tuttlingen, Germany).

Locally established four cell lines were isolated from two HNSCC patients, having both primary and metastatic tumors. Details of the cell lines are provided in supplementary Table 1.

Preparation of the wells and light microscope imaging of cell morphology

Ninety-six-well plates with black well walls and clear bottoms (Essen Bioscience, Ann Arbor, MI, USA) were used for coating. The plate was placed on ice and 50 µL/well of 0.5 mg/mL Matrigel and collagen (Corning, Corning, NY, USA) were dispensed using cold pipet tips. The plate was placed in the incubator for 30 minutes, then 50 µL/well of 0.01mg/mL BSA (Sigma-Aldrich), 0.01 mg/mL fibronectin (Sigma-Aldrich), 0.5 mg/mL Myogel (Lab made, see below), and 0.5mg/mL fibrin (For fibrin preparation, see below) was added to the plate. The plate was incubated at the cell culture incubator for overnight. Cells were detached from flasks using trypsin-EDTA and seeded at the density of 1000 cells/well in 100 µL of complete medium.

Myogel was prepared from human uterus leiomyoma tissue following the instructions in Salo et al., 2015 (8). Briefly, tissue pieces were frozen using liquid nitrogen and crushed into a powder

with CryoMill (Retsch, Haan, Germany). A volume of 20 ml of ice cold NaCl buffer (3.4 M, pH 7.4) was mixed with 10 g of tissue powder and centrifuged. 20 ml of the same NaCl buffer was used to homogenize the pellet with a T18 Ultra-Turrax (IKA®-Werke GmbH & Co. KG, Staufen, Germany). DC Protein Assay (Bio-Rad, Hercules, California, United States) was used to measure the protein concentration in each preparation. The Myogel solution was stored in small (≤1 ml) aliquots at −20 °C.

Fibrin was prepared using 0.5 mg/mL fibrinogen (Merck, Darmstadt, Germany), 33,3 µg/mL aprotinin (Sigma-Aldrich) and 0,34 U/mL thrombin (Sigma-Aldrich).

To observe the effect of matrices on cell morphology, pictures of each well were taken after 3 days using the reverse Nikon Digital sight DS-U3 microscope (Nikon, Tokyo, Japan) at x10 and x20 magnification.

Scanning electron microscope assay

We used two cell lines (UT-SCC-42A and UT-SCC-42B) to study the cell-matrix interaction under scanning electron microscope. Glass coverslips were inserted into wells of a 24 well plate (Corning) and coated using 300 µL of coating suspension (using the same concentrations as above for each matrix). Six thousand cells were seeded on each coverslip and incubated for 2 days. For fixation, we performed several washing steps with 500 µL of phosphate-buffered saline (PBS), and then we added 500 µL of 4% formaldehyde and kept it for 20 minutes at room temperature. After that, we washed the wells with PBS again for 3 times, 5 minutes each. Samples were dehydrated using graded ethanol series and dried using K850 critical point dryer (Quorum Technologies, UK). After drying, samples were attached to aluminium stubs with double-sided carbon tape and coated with 5 nm of platinum using Q150T ES sputter coater (Quorum Technologies, UK). Samples were imaged with Sigma HD-VP field-emission scanning electron microscope (Carl Zeiss, Oberkochen, Germany).

Proliferation luminescent cell viability assay

For proliferation, we used the same experiment settings as in the imaging assay. After 3 days, the plate was taken out from the incubator to room temperature for 15 min before starting the assay. 100 µL of CellTiter-Glo was dispensed in each well. The plate was put on a plate shaker (Heidolph,

Schwabach, Germany) for 5 min at 450 rpm and then in plate spinner (Thermo Scientific, Massachusetts, USA) for 5 min at 1000 rpm. Finally, the plate was placed in the BMG PHERAstar FS (BMG Labtech, Offenburg, Germany) plate reader to detect cell viability.

Scratch wound cell migration assay

The same coating protocol was used as before, except that the gels were sucked out before seeding the cells. We seeded the cells at the following density: 25000/well for UT-SCC-24A and UT-SCC-42B and 30000/well for UT-SCC-24B and UT-SCC-42A. Matrigel was not used in this experiment as the cells were forming clusters on top of the Matrigel leading to difficulties in getting a smooth scratch. The wound maker (Essen Bioscience) was used to achieve homogeneous scratch wounds.

Wounds were checked under the light microscope and the media was changed for all the wells. The plate was placed in IncuCyte ZOOM incubator (Essen Bioscience), and wounds confluences were monitored using the IncuCyte Live-Cell Imaging System (Essen Bioscience). Images were taken each hour for 20 hours. Supplementary Video (Online Resource 1) shows the migration of the UT-SCC-42A cells on top of Myogel.

Scratch wound cell invasion assay

Four gels were used in this experiment: collagen, Myogel-collagen, fibrin, and Myogel-fibrin at the concentration of 1 mg/mL for all of them, as instructed by the manufacturer (Essen Bioscience). Similar to the migration experiment, wells were coated, cells were seeded and a scratch wound was made. After that, 50 µL of the gels were added. Once the gels solidified, 50 µL of media was added. The plate was placed in IncuCyte ZOOM incubator, and wounds confluences were monitored using the IncuCyte Live-Cell Imaging System (Essen Bioscience). Images were taken each hour for 48 hours. Supplementary Video (Online Resource 2) shows the invasion of the UT-SCC-42A within Myogel-collagen.

Spheroid Invasion Assay

Cells were seeded at the concentration of 1000 cells/well in 50 µL using ultra-low attachment 96-well round bottom plate wells (Corning). The plate was incubated for 4 days to allow spheroid

formation. Spheroids were embedded in 100 µL of Matrigel (0.5 mg/mL), collagen (0.5 mg/mL), Myogel-collagen (0.5 mg/mL), fibrin (0.5 mg/mL fibrinogen + 0.3 U/mL Thrombin + 3.33 mg/mL Aprotinin), and Myogel-fibrin (0.5 mg/mL). Gels were allowed to solidify for 30 minutes and then 100 µL of DMEM was added into each well. The plate was incubated for 4 days and pictures were taken every day using Nikon Digital sight DS-U3 microscope (Nikon) at x4 magnification. The used protocol is explained in detail in Naakka et al., 2019 (9). We analyzed the area covered by cells using ilastik and ImageJ (Wayne Rasband, National Institute of Mental Health, Bethesda, MD, USA). Once ilastik detected area covered by cells, we used a custom plugin, written for ImageJ, to measure the area. The plugin converts the image to black and white image. All pixels outside the area are set to zero, the cells area is set to one. The total area is measured as a number of pixels equal to one.

Microarray

UT-SCC-24A and UT-SCC-24B cell lines were used to study the effects of different matrices on the molecular gene profile using RNA sequencing transcriptome profiles. Wells of 24 well-plates were coated with 150 µL of gels (using the same concentrations as in the imaging assay) and seeded with 150 000 cells. Cells were left on the gels for 24 hours and lysed using RLT buffer. RNA was extracted using RNeasy Kit (Qiagen, Düsseldorf, Germany) according to manufacturer instructions. In case some clots or fragments of gels existed in the cell lysate, sonication was used to solubilize them. The quality of total RNA was assessed with a TapeStation (Agilent Technologies, Santa Clara, CA, USA), and only samples of high quality (RNA integrity value >8) were included in the analyses. The starting amount of total RNA was 100 ng. The labeling and hybridization were done according to the manufacturer's instructions by using Applied Biosystems GeneChipTM WT PLUS Reagent Kit and Manual Target Preparation for GeneChipTM Whole Transcript (WT) Expression Arrays (UserGuide 23 January 2017; Thermo Fisher Scientific). Fifteen micrograms of cRNA were used for single-stranded cDNA-synthesis (sscDNA) and a total of 5,5 ug of sscDNA was fragmented. A total of 2.3 µg was hybridized on Clariom S Affymetrix array.

Gene set enrichment and pathway analysis

Gene set enrichment analysis (GSEA, http://software.broadinstitute.org/gsea/index.jsp) (13) was carried out to connect gene expression signatures with previously known gene sets and pathways.

The analysis was performed for each cell line and matrix combination separately using the full expression data set against C2: curated gene sets available at broad institute web page. Genes were ranked using signal-to-noise ratio and gene set permutation was used for FDR estimation and enrichment score adjustment. Additional analyses for Gene Ontology enrichment and KEGG pathway visualization were carried out in R (v. 3.5.3) using packages gage (generally applicable gene set enrichment, v. 2.32.1) (14) and pathview (v. 1.22.3) (15). Both the GSEA and additional R analyses were performed by the Functional Genomics Unit (FuGU) at the University of Helsinki. Two samples (UT-SCC-24A/fibrin and UT-SCC-24B/fibrin) were excluded from the analysis as a result of probability of mislabelling.

Analysis of cell circularity and their surface area

Cell circularity and surface area were measured using ImageJ software (Wayne Rasband, National Institute of Mental Health, Bethesda, MD, USA). The experiments were done four times independently. Two wells were used for each condition and 3 cells were randomly selected and measured from each well.

Statistical analysis

All experiments were repeated independently at least three times, each in duplicate or triplicate. Values are given as means ± standard deviations. All statistical analyses were performed using SPSS (IBM SPSS Statistics for Windows, version 21.0; Armonk NY, IBM Corp.) To determine the statistical significance, we performed one-way analysis of variance (ANOVA) followed by Bonferroni correction. We set statistical significance to $p<0.05$. P values were presented as follows: * = $P \leq 0.05$, ** = $P \leq 0.01$, *** = $P \leq 0.001$, **** = $P \leq 0.0001$. Origin lab software was used to create the figures.

Results:

SCC cell morphology is affected by the matrix type

Cancer cell morphology was affected by the type of matrix (Figure 1). While cells seeded on BSA had similar morphology to the cells in the control wells, cells on Matrigel formed round clusters.

Cells on fibronectin had a more flattened surface than cells on the other matrices. Cells on Myogel, fibrin, and collagen were more spindle in shape and there were fibers surrounding the cells. Here we present the pictures of UT-SCC-24B cells only since the other cell lines behaved similarly (data not shown).

For all the cell lines, cells on Matrigel had the highest circularity value (above 0.8 out of 1) due to the formation of cell clusters, though circularity was close to 0.8 in many instances with the other matrices as well (Figure 2).

The majority of the cell lines, except UT-SCC-24A, seeded on top of fibronectin had higher surface area than in the other conditions, but this difference did not reach statistical significance (Figure 3). UT-SCC-24A cultured on top of fibrin had significantly lower surface area compared to the cells on plastic wells (Figure 3).

Cell-matrix interaction

Scanning electron microscope was used to observe the differences between structures of matrices (Figure 4). While Matrigel has a fiber sheet structure, Myogel's structure was in form of thin unorganized fibers together with small globular proteins. Fibrin has abundant thin fibers. Collagen presented helical fibers structure. Fibronectin did not show a fibril structure.

The SEM pictures revealed the interaction between the cells and the matrices (Figure 5). Cells cultured on BSA behaved similarly to the controls. On top of Matrigel, cells formed small clusters. Cells on fibronectin tend to be flat with large surface areas. As for Myogel, cells were gathered in groups and they were in contact with several fibers. For fibrin and collagen, cells were embedded within the matrix fibers.

Fibrin increased and collagen reduced SCC proliferation, while matrix effect on cell migration was cell line dependent.

The proliferation rate for all the tested cell lines was the highest on top of fibrin, and the lowest on top of collagen (Figure 6). This difference was significant for the fibrin-coated wells in case of UT-SCC-24A, 24B, and 42A, and for the collagen-coated wells in case of UT-SCC-24A and 42A.

The scratch wound cell migration assay showed that some matrices were able to affect cancer cell migration but this effect was cell line-dependent (Figure 7). Opposite to the proliferation results, collagen induced UT-SCC-24B migration and fibrin reduced it. For UT-SCC-42A, cells cultured on top of Myogel were migrating significantly slower compared to the control. Matrigel was not used for migration assay since the cells formed clusters and a homogeneous wound was not possible to be achieved.

Myogel induced SCC cell invasionCancer cells had different invasion speeds in the scratch wound invasion assay based on the matrix used (Figure 8). Cells cultured within Myogel-collagen invaded the fastest. On the other hand, cells did not invade through Myogel-fibrin and fibrin matrices. Myogel was able to induce cancer cell invasion when added to the collagen significantly in case of UT-SCC--42 A and B.

For UT-SCC-24A, 42A, and 42B, Myogel-fibrin matrix was the best to induce the spheroid invasion followed by Myogel-collagen (Figure 9, Figure 10). UT-SCC-24B invaded the fastest in Myogel-collagen followed by Myogel-fibrin (Figure 10). Myogel was able to significantly induce cancer cell invasion when added to the fibrin in case of UT-SCC-24B and 42A (Figure 10).

Fibrin had the highest and BSA and fibronectin the lowest impact on SCC cell molecular profile

In order to understand the mechanism behind the effect of different matrices on the SCC cells behavior, we studied the molecular gene profile using RNA sequencing transcriptome profiles. Matrices were able to change the gene expression of hundreds of genes (Supplementary Table 2). While cells seeded on fibrin had the largest difference (574 and 103 genes significantly affected, $P \leq 0.05$, in UTSCC-24A and B, respectively), cells on BSA (15 and 19 genes significantly affected in UTSCC-24A and B, respectively) and fibronectin (9 and 15 genes significantly affected in UTSCC-24A and B, respectively) showed the least difference in their genes expression compared with the cells cultured on plastic (Supplementary Table 2). The most significantly affected genes for each matrix are presented in Supplementary Table 3.

Gene ontology enrichment analysis revealed several affected ontology groups (Supplementary Table 4). These were both matrix and cell line dependent. The 10 most up- and downregulated biological processes indicated by analysis are presented in Supplementary Table 5.

Due to the large variation between the two cell lines, we unfortunately were not able to detect specific genes or ontology groups directly responsible for the changes in the SCC cells behavior.

Discussion

ECMs are increasingly used in cancer research to study different aspects of cancer cell behavior, such as proliferation, migration, invasion and drug testing. The usage of these matrices was regarded as a leap in moving closer to *in vivo* conditions than the traditional 2D cell culture on plastic. This is mainly due to the ability of these matrices to provide essential elements needed for the cell-cell and cell-matrix interaction. Due to the presence of several types of ECM, such as Matrigel, Myogel, collagen, and fibrin, choosing the most suitable matrix that fits with the needed assays without knowing its properties and effects could be risking the reliability of the results . Unfortunately, several researchers select the matrix type for their assay based only on the availability, cost, and easiness of the matrix handling, without paying attention to the effect of the matrix on cancer cell behavior. Using a non-representative tumor matrix could lead to non-reliable results. In this project, we pointed out the significant differences in SCC cells behavior and their gene profile when tested with various matrices. This emphasizes the importance of selecting the most suitable matrix for each assay.

We first studied the effect of five matrices on the HNSCC cell morphology. Interestingly, all the used cell lines formed cell round clusters when cultured on top of Matrigel, which is the most common commercial extracellular matrix used in *in vitro* experiments. Our results are in line with several other studies showing similar cell behavior on Matrigel in different cancer types (16-18). Forming cell clusters may be due to the presence of a large amount of basement membrane proteins in Matrigel which seems to hold the cells together (19). Even though mimicking the basement membrane is considered as an advantage for Matrigel, this feature is a disadvantage in invasion assays due to the difficulties of cancer cells to invade through it. Opposite to the Matrigel, cells cultured on top of Myogel, fibrin and collagen had a spindle shape, which represents more the invasive phenotype of carcinoma cells, as reported in several publications (16,20,21). This

morphology may represent an epithelial-mesenchymal transition (EMT), which is an important feature for cancer cell migration and invasion (22-24). Cells cultured on fibronectin had a unique flattened shape with a large surface area. This shape could be explained by the presence of the $\alpha_5\beta_1$ integrin (25) which is a fibronectin receptor (26), leading to an interaction that requires traction forces provided by the matrix.

To confirm our visual observation of cell morphology, we measured the circularity and surface area of the cells. As expected, cells cultured on top of Matrigel had the highest circularity value due to the formation of round clusters. On the other hand, cells cultured on fibronectin had the highest surface area due to the flat shape of the cells.

In order to get a better understanding of the cell-matrix interaction, we visualized the cells and the matrix under scanning electron microscope. As expected, most of the used matrices, except BSA and fibronectin, have fibril structures. The fibril structure of the matrices differed from one matrix to another in the terms of the amount of the fibers (rich *vs* poor) and thickness of the fibers (thick *vs* thin). All these differences, in addition to the presence or absence of several growth factors and other proteins, explain the differences in the behavior of cancer cells from one matrix to another. The interaction between the cells and the matrix was also different from one matrix to another. For some matrices, as in Myogel, the cells were surrounded by fibers, while for others, cells were either on top of the matrix (Matrigel) or embedded in it (fibrin and collagen).

As cell viability assay is one of the main assays used in *in vitro* cancer research, we studied if the matrix itself could have an effect on cancer cell proliferation. Interestingly, one pattern was found in all the tested cell lines with the highest proliferation rate detected in the fibrin-coated wells and the lowest in the collagen wells. Our results are in line with Simpson-Haidaris *et al*. who reported similar results for breast cancer cells MCF-7 cultured on fibrin (27). On the other hand, our results are opposite to Chen *et al*., who reported a higher proliferation rate of MCF-7 cells when cultured on a porous collagen scaffold (28), suggesting that the effect of the collagen matrix is cell line dependent. Other matrices did not have a significant effect on HNSCC cell proliferation which goes hand by hand with some studies (29,30).

Next, we studied the effect of the different matrices on cancer cell migration. Our results revealed that the effects of the studied matrices on HNSCC migration were cell line dependent, and the significant effects were assured by collagen, Myogel, and fibrin for some cell lines. It was an interest to us to notice the opposite effect of collagen and fibrin matrices on the

proliferation and migration behavior of the UT-SCC-24B cell line. While these cells had the highest rate of proliferation on fibrin and the lowest on collagen, the opposite happened in cell migration. This may return to the fact that the low proliferative cancer cells have high migration capacity and *vice versa* (31).

Our scratch wound cell invasion assay showed that cells cultured within Myogel-collagen 3D matrix invaded faster than cells within other matrices. This induction of invasion was mainly due to Myogel since we also cultured HNSSC cells within collagen alone and the invasion speed was lower. A similar effect of Myogel was observed on other cell lines (1). Cancer cells did not invade through fibrin or Myogel-fibrin, which may be due to the fibrin's compact structure.

Similar to scratch wound cell invasion assay, Myogel was able to induce invasion in spheroids. However, in scratch wound assay, Myogel-collagen was the most invasive inductive matrix in all 4 cell lines, while in spheroid 3 out of 4 cell lines invaded fastest in Myogel-fibrin and one in Myogel-collagen. This difference is most likely due to differences in the concentration of the gels in the two assays (1 mg/ml in the scratch wound invasion and 0.5 mg/ml in the spheroid invasion assays). Gels concentration were choosen either following the manufacturer instruction (scratch wound invasion assay) or after lab optimization (spherioid invasion assay). Based on both invasion assays, adding Myogel seems to improve the speed of HNSCC cancer cell invasion. This Myogel property could help in studying low invasive cancer cell lines and testing anti-invasive cancer treatments.

Matrigel has been the mostly used matrix for *in vitro* 3D cancer research. However, it should be kept in mind that it is derived from mouse sarcoma containing mostly basement membrane proteins (19). Due to its nature, in our invasion assays, cells failed to invade efficiently.

Based on our mRNA microarray results, the matrix type was able to significantly affect hundreds of genes and several pathways. Interestingly, these genes and pathways were not shared between matrices or cell lines but were matrix and cell line dependent. This was the reason that unfortunately we were not able to detect specific gene or pathway responsible for the changes in the SCC cells behavior. These results indicate that one cell line cannot represent the behavior of any studied tumor type, and always more than one cell line should be used in *in vitro* experiments.

Our study revealed important effects of the ECMs on HNSCC cells' behavior, morphology, and molecular gene profile. We showed here that the ECMs are not idle elements, but instead, they have significant effects on the *in vitro* results. We believe that for each assay, selecting the

appropriate matrix, based on its characteristics and the studied cell line, is necessary to get reliable results in *in vitro* experiments. In theory, selecting human tumor-derived matrix could represent the closest condition to the *in vivo* tumor microenvironment which increases the reliability of the *in vitro* cancer cells testing.

Acknowledgment:

We acknowledge the funders of this study: the Sigrid Jusélius Foundation, The Cancer Society of Finland, Oulu University Hospital MRC grant, the Emil Aaltonen Foundation, Helsinki University Central Hospital Research Funds, and Jane and Aatos Erkkos Foundation.

References:

(1) Salo T, Dourado MR, Sundquist E, Apu EH, Alahuhta I, Tuomainen K, et al. Organotypic three-dimensional assays based on human leiomyoma–derived matrices. Philosophical Transactions of the Royal Society B: Biological Sciences 2018;373(1737):20160482.

(2) Whittaker CA, Bergeron K, Whittle J, Brandhorst BP, Burke RD, Hynes RO. The echinoderm adhesome. Developmental Biology 2006;300(1):252-266.

(3) Provenzano PP, Eliceiri KW, Campbell JM, Inman DR, White JG, Keely PJ. Collagen reorganization at the tumor-stromal interface facilitates local invasion. BMC Medicine 2006;4(1):38.

(4) Sundquist E, Renko O, Salo S, Magga J, Cervigne NK, Nyberg P, et al. Neoplastic extracellular matrix environment promotes cancer invasion in vitro. Experimental cell research 2016;344(2):229-240.

(5) Lu P, Weaver VM, Werb Z. The extracellular matrix: A dynamic niche in cancer progression. Journal of Cell Biology 2012;196(4):395-406.

(6) Quante M, Tu SP, Tomita H, Gonda T, Wang SSW, Takashi S, et al. Bone Marrow-Derived Myofibroblasts Contribute to the Mesenchymal Stem Cell Niche and Promote Tumor Growth. Cancer Cell 2011;19(2):257-272.

(7) Lou Y, Kanninen L, Kuisma T, Niklander J, Noon LA, Burks D, et al. The Use of Nanofibrillar Cellulose Hydrogel As a Flexible Three-Dimensional Model to Culture Human Pluripotent Stem Cells. Stem Cells and Development 2014;23(4):380-392.

(8) Salo T, Sutinen M, Hoque Apu E, Sundquist E, Cervigne NK, de Oliveira CE, et al. A novel human leiomyoma tissue derived matrix for cell culture studies. BMC Cancer 2015;15(1):981.

(9) Naakka E, Tuomainen K, Wistrand H, Palkama M, Suleymanova I, Al-Samadi A, et al. Fully Human Tumor-based Matrix in Three-dimensional Spheroid Invasion Assay. Journal of Visualized Experiments 2019(147):e59567.

(10) Al-Samadi A, Poor B, Tuomainen K, Liu V, Hyytiäinen A, Suleymanova I, et al. In vitro humanized 3D microfluidic chip for testing personalized immunotherapeutics for head and neck cancer patients. Experimental Cell Research 2019;383(2):111508.

(11) Almahmoudi R, Salem A, Murshid S, Dourado RM, Apu HE, Salo T, et al. Interleukin-17F Has Anti-Tumor Effects in Oral Tongue Cancer. Cancers 2019;11(5).

(12) Tuomainen K, Al-Samadi A, Potdar S, Turunen L, Turunen M, Karhemo P, et al. Human Tumor–Derived Matrix Improves the Predictability of Head and Neck Cancer Drug Testing. Cancers 2019;12(1).

(13) Subramanian A, Tamayo P, Mootha VK, Mukherjee S, Ebert BL, Gillette MA, et al. Gene set enrichment analysis: A knowledge-based approach for interpreting genome-wide expression profiles. Proceedings of the National Academy of Sciences USA 2005;102(43):15545.

(14) Luo W, Friedman MS, Shedden K, Hankenson KD, Woolf PJ. GAGE: generally applicable gene set enrichment for pathway analysis. BMC Bioinformatics 2009;10(1):161.

(15) Luo W, Brouwer C. Pathview: an R/Bioconductor package for pathway-based data integration and visualization. Bioinformatics 2013;29(14):1830-1831.

(16) Truong D, Puleo J, Llave A, Mouneimne G, Kamm RD, Nikkhah M. Breast Cancer Cell Invasion into a Three Dimensional Tumor-Stroma Microenvironment. Scientific Reports 2016;6(1):34094.

(17) Beers J, Gulbranson DR, George N, Siniscalchi LI, Jones J, Thomson JA, et al. Passaging and colony expansion of human pluripotent stem cells by enzyme-free dissociation in chemically defined culture conditions. Nature Protocols 2012;7(11):2029-2040.

(18) Polo ML, Arnoni MV, Riggio M, Wargon V, Lanari C, Novaro V. Responsiveness to PI3K and MEK Inhibitors in Breast Cancer. Use of a 3D Culture System to Study Pathways Related to Hormone Independence in Mice. PLOS ONE 2010;5(5):e10786.

(19) Zhang Y, Lukacova V, Reindl K, Balaz S. Quantitative characterization of binding of small molecules to extracellular matrix. The Journal of Biochemical and Biophysical Methods 2006;67(2):107-122.

(20) Chen Y, Lan H, Wu Y, Yang W, Chiou A, Yang M. Epithelial-mesenchymal transition softens head and neck cancer cells to facilitate migration in 3D environments. Journal of Cellular and Molecular Medicine 2018;22(8):3837-3846.

(21) Hakkinen KM, Harunaga JS, Doyle AD, Yamada KM. Direct Comparisons of the Morphology, Migration, Cell Adhesions, and Actin Cytoskeleton of Fibroblasts in Four Different Three-Dimensional Extracellular Matrices. Tissue Engineering Part A 2011;17(5-6):713-724.

(22) Son H, Moon A. Epithelial-mesenchymal Transition and Cell Invasion. Toxicological research 2010;26(4):245-252.

(23) Kalluri R, Weinberg RA. The basics of epithelial-mesenchymal transition. Journal of Clinical Investigation 2009;119(6):1420-1428.

(24) Zhou P, Li B, Liu F, Zhang M, Wang Q, Liu Y, et al. The epithelial to mesenchymal transition (EMT) and cancer stem cells: implication for treatment resistance in pancreatic cancer. Molecular Cancer 2017;16(1):52.

(25) Ahmedah HT, Patterson LH, Shnyder SD, Sheldrake HM. RGD-Binding Integrins in Head and Neck Cancers. Cancers 2017;9(6):56.

(26) Wang K, Seo BR, Fischbach C, Gourdon D. Fibronectin Mechanobiology Regulates Tumorigenesis. Cellular and molecular bioengineering 2016;9:1-11.

(27) Simpson-Haidaris P, Rybarczyk B. Tumors and Fibrinogen. Annals of the New York Academy of Sciences 2001;936(1):406-425.

(28) Chen L, Xiao Z, Meng Y, Zhao Y, Han J, Su G, et al. The enhancement of cancer stem cell properties of MCF-7 cells in 3D collagen scaffolds for modeling of cancer and anti-cancer drugs. Biomaterials 2012;33(5):1437-1444.

(29) Hurst RE, Kyker KD, Bonner RB, Bowditch RD, Hemstreet,George P.,,3rd. Matrix-dependent plasticity of the malignant phenotype of bladder cancer cells. Anticancer Research 2003 Jul;23(4):3119-3128.

(30) Fliedner FP, Hansen AE, Jørgensen JT, Kjær A. The use of matrigel has no influence on tumor development or PET imaging in FaDu human head and neck cancer xenografts. BMC Medical Imaging 2016;16(1):5.

(31) Mouneimne G, Brugge JS. YB-1 Translational Control of Epithelial-Mesenchyme Transition. Cancer Cell 2009;15(5):357-359.

Figure legends:

Figure 1. SCC cell morphology observed under light microscope. Different shapes of UT-SCC-24B cells were observed depending on the used matrix. Cells on BSA gave similar morphology to the control. Cells were clustered on Matrigel, flat on fibronectin, and spindle on Myogel, fibrin, and collagen. Scale bar = 100 µm

Figure 2. SCC cell circularity. UT-SCC cells were cultured on different matrices and plastic (control) for 3 days and pictured on day 3 under light microscope. Cell circularity was measured using ImageJ software. In all cell lines represented in the figure, cells cultured on top of Matrigel showed the highest circularity value (above 0.8). Data are presented as means ± standard deviations.* $P \leq 0.05$. N=3.

Figure 3. SCC cell surface area. UT-SCC cells were cultured on different matrices and plastic (control) for 3 days and pictured on day 3 under light microscope. Cell surface area was measured using ImageJ software. UT-SCC-24B, UT-SCC-42A and UT-SCC-42B cells showed the highest cell surface area when cultured on Fibronectin, but this difference did not reach statistical significance. Data are presented as means ± standard deviations.* $P \leq 0.05$. N=3.

Figure 4. Matrices structure observed under scanning electron microscope. Coverslips were coated with different matrices and prepared for scanning electron microscope. Matrigel has a fiber sheet structure. Myogel's structure was in form of thin unorganized fibers together with

small globular proteins. As for fibrin, its fibers were thin. Collagen presented helical fibers structure. BSA and fibronectin did not show a fibril structure. Scale bar = 1 µm

Figure 5. SCC cells and matrix interaction observed under scanning electron microscope. UT-SCC 42B cells were cultured on coated coverslips with different matrices and prepared for scanning electron microscope. Cells cultured on BSA coated wells did not have any interaction with the matrix, similarly to the cells cultured on plastic. For Matrigel, cells formed small clusters on top of the matrix. Cells on fibronectin tend to be flat, more than any studied matrix, with a large surface area. As for Myogel, cells were gathered in groups and they were in contact with several fibers. In fibrin and collagen, cells were embedded within the matrix fibers. Scale bar = 10 µm

Figure 6. SCC cell proliferation rate on different matrices. UT-SCC cells were cultured on different matrices for three days and the cell proliferation rate was measured using luminescent cell viability assay. The proliferation rate for all the cell lines was the highest on fibrin and the lowest on collagen. This difference was significant for the fibrin-coated wells in case of UT-SCC-24A, 24B, and 42A cell lines and also for collagen in case of UT-SCC-24A and 42A cell lines. The red line represents the control value. Data are presented as means ± standard deviations.* $P \leq 0.05$, ** ≤ 0.01, *** ≤ 0.001, **** ≤ 0.0001. N=3

Figure 7. SCC cell migration on different matrices. UT-SCC cells were cultured on different matrices and cell migration was evaluated using scratch wound cell migration assay. The migration rate was dependent on both the matrix and the cell line. Data are presented as migration curves and area under the curves as means ± standard deviations.* $P \leq 0.05$, ** ≤ 0.01, *** ≤ 0.001, **** ≤ 0.0001. N=3.

Figure 8. SCC cell invasion through different matrices. UT-SCC cells were cultured on different matrices and cell invasion was evaluated using scratch wound cell invasion assay. The four studied cell lines showed the fastest invasion rate when cultured on Myogel-collagen and they did not invade through fibrin and Myogel-fibrin. Data are presented as invasion curves and area under the curves as means ± standard deviations.* ≤ 0.05, ** ≤ 0.01, *** ≤ 0.001, **** ≤ 0.0001. N=3.

Figure 9. Spheroid invasion observed under light microscope. UT-SCC 42A cells were cultured in ultra-low attachment 96-well round bottom plate wells and embedded in different matrices. Spheroids were observed under light microscope. Scale bar = 100 µm.

Figure 10. SCC spheroid invasion though different matrices. UT-SCC cells were cultured in ultra-low attachment 96-well round bottom plate wells and embedded in different matrices. For UT-SCC-24A, 42A, and 42B, Myogel-fibrin matrix showed the fastest spheroids invasion, followed by Myogel-collagen. For UT-SCC-24B cells invaded faster in Myogel-collagen followed by Myogel-fibrin. Data are presented as invasion curves and area under the curves as means ± standard deviations. *≤0.05, *** ≤ 0.001, **** ≤ 0.0001. N=3.

List of Supporting Information:

Supplementary Table 1. HNSCC cell lines details. Clinical and pathological characteristics of the HNSCC cell lines. TNM is based on

Supplementary Table 2. Number of differentially expressed genes of UT-SCC-24A and B cultured on different matrices. Results of mRNA microarray showing the number of differentially expressed genes between cells cultured on plastic and cells cultured on matrices. The genes that passed the filter criteria had a $p<0.05$ and a fold change ≤-2 or ≥2. Transcriptome analysis console software was used to analyze the data

Supplementary Table 3. The most affected genes of UT-SCC cells cultured on different matrices. Results of mRNA microarray showing the most significantly affected genes (up- down-regulated) by each matrix we used. The genes that passed the filter criteria had a $p<0.05$ and a fold change ≤-2 or ≥2. Transcriptome analysis console software was used to analyze the data.

Supplementary Table 4. Number of differentially expressed pathways of UT-SCC-24A and B cultured on different matrices. Results of the gene set enrichment analysis (GSEA) showing the number of the differentially represented pathways between cells cultured on plastic and cells cultured on matrices. The pathways that passed the filter criteria had a $p<0.05$.

Supplementary Table 5. The 10 most affected pathways of UT-SCC cells cultured on different matrices. Results of the gene set enrichment analysis (GSEA) showing the 10 most differentially expressed pathways between cells cultured on plastic and cells cultured on matrices. The pathways that passed the filter criteria had a $p<0.05$.

548 **Supplementary video 1:** migration of the UT-SCC-42A cells on top of Myogel.

549 **Supplementary video 2:** the invasion of the UT-SCC-42A within Myogel-collagen.

550

551

552

553

Supplementary table 1: HNSCC cell lines details. Clinical and pathological characteristics of the HNSCC cell lines. TNM is based on pathology report.

Patients	1		2	
Cell line	UT-SCC-24A	UT-SCC-24B	UT-SCC-42A	UT-SCC-42B
Origin	Tongue SCC Primary Tumor	Tongue SCC Metastatic lymph node	Laryngeal SCC Primary Tumor	Laryngeal SCC Metastatic lymph node
Sex	Male			
Age	41		43	
Classification	T2N0M0	T2N1M0	T4N3M0	
Grade	2		3	
Environmental risk factors	- Alcohol - smoking			

Supplementary table 2: Number of differentially expressed genes of UT-SCC 24A and B cultured on different matrices. Results of mRNA microarray showing the number of differentially expressed genes between cells cultured on plastic and cells cultured on matrices. The genes that passed the filter criteria had a $p<0.05$ and a fold change ≤ -2 or ≥ 2. Transcriptome analysis console software was used to analyze the data

Cell line /Matrix	Number of genes which passed the filter criteria	Up-regulated	Down-regulated
UTSCC-24A/ BSA	15	4	11
UTSCC-24A/ Matrigel	207	70	137
UTSCC-24A/ Fibronectin	9	3	6
UTSCC-24A/ Myogel	151	62	89
UTSCC-24A/ Fibrin	574	284	290
UTSCC-24A/ Collagen	43	26	17
UTSCC-24B/ BSA	19	13	6
UTSCC-24B/ Matrigel	31	23	8
UTSCC-24B/ Fibronectin	15	12	3
UTSCC-24B/ Myogel	12	9	3
UTSCC-24B/ Fibrin	103	76	27
UTSCC-24B/ Collagen	52	24	28

Supplementary table 3: The most affected genes of UT-SCC cells cultured on different matrices. Results of mRNA microarray showing the most significantly affected genes (up- down-regulated) by each matrix we used. The genes that passed the filter criteria had a $p<0.05$ and a fold change ≤ -2 or ≥ 2. Transcriptome analysis console software was used to analyze the data.

UTSCC-24A BSA							
UP				DOWN			
Gene	Fold change	P.Val	FDR P.Val	Gene	Fold change	P.Val	FDR P.Val
BEST2	2,76	0,0006	0,9453	ZNF254	-2,08	0,0022	0,9606
OSBPL7	2,55	0,0030	0,9606	ST5	-2,02	0,0027	0,9606
CXCL10	2,2	0,0085	0,9996	EPB41	-2,16	0,0033	0,9606
EPN3	2,06	0,0149	0,9996	KIF5C	-2,04	0,0053	0,9996
				RBMS1	-2,01	0,0131	0,9996
				ZNF91	-2,12	0,0133	0,9996
				RBM26	-3,12	0,0149	0,9996
				BIRC6	-2,03	0,0245	0,9996
				KIDINS220	-2,09	0,0285	0,9996
				HDAC9	-2,07	0,0471	0,9996

UTSCC-24A Matrigel							
UP				DOWN			
Gene	Fold change	P.Val	FDR P.Val	Gene	Fold change	P.Val	FDR P.Val
CCL20	6,25	6,07E-08	0,0003	TGFB2; TGFB2-OT1	-4,13	1,50E-08	0,0002
ALG3	2,23	2,38E-06	0,0032	GADD45A	-2,26	1,13E-07	0,0005
FOSL1	3,5	2,98E-06	0,0033	MAP2	-2,56	1,28E-07	0,0005
ETV5	2,54	3,88E-06	0,0033	PDZD2	-2,61	4,18E-07	0,0009
C6orf136	2,11	4,56E-06	0,0036	TPM1	-2,55	5,89E-07	0,0011
SH2B3	2,58	7,02E-06	0,0046	PLK2	-2,11	1,14E-06	0,0019
TGIF2	2,1	9,66E-06	0,0052	ABHD4	-2,06	6,13E-06	0,0042
LYAR	2,1	2,12E-05	0,0079	SCARA3	-2,4	8,26E-06	0,0048
PHLDA1	3,29	2,25E-05	0,0079	JPH2	-2,73	9,01E-06	0,0051
CHCHD10	2,32	2,27E-05	0,0079	RND3	-2,07	1,41E-05	0,0063

UTSCC-24A Fibronectin							
UP				DOWN			
Gene	Fold change	P.Val	FDR P.Val	Gene	Fold change	P.Val	FDR P.Val
NPVF	2,11	0,0057	0,9988	ST3GAL3	-2,05	0,0002	0,9988
RFX3	2,08	0,0128	0,9988	ST5	-2,14	0,0110	0,9988
NUPR1	2,02	0,0147	0,9988	NPY4R	-2,06	0,0233	0,9988
				PLCE1	-2,47	0,0304	0,9988
				DNAH5	-2,47	0,0373	0,9988
				ADAMTS7	-2,47	0,0403	0,9988

UTSCC-24A Myogel							
UP				DOWN			
Gene	Fold change	P.Val	FDR P.Val	Gene	Fold change	P.Val	FDR P.Val
MARCH4	2,44	6,39E-08	0,0008	OLR1	-4,38	2,61E-06	0,0049
SLC29A1	2,21	7,10E-08	0,0008	GATS	-2,62	6,92E-06	0,0069
HMGA2	2,93	1,47E-07	0,0008	ATF7IP2	-2,21	9,70E-06	0,0090
ETV5	3,76	2,20E-07	0,0009	TMEM52B	-3,09	1,64E-05	0,0122
LRRC8C	2,47	7,06E-07	0,0025	MTUS1	-2,22	1,80E-05	0,0129
DCTPP1	2,01	8,35E-07	0,0026	PLAC8	-3,82	2,16E-05	0,0131
CGB5; CGB8	2,31	2,20E-06	0,0047	BIRC3	-2,48	2,22E-05	0,0131
CDC42EP2	2,81	2,72E-06	0,0049	TRANK1	-2,29	3,76E-05	0,0175
HGH1	2,21	4,31E-06	0,0059	REL	-2,11	5,99E-05	0,0211
MARC1	2,18	4,70E-06	0,0059	MUC16	-4,08	0,0001	0,0311

UTSCC-24A Fibrin							
UP				DOWN			
Gene	Fold change	P.Val	FDR P.Val	Gene	Fold change	P.Val	FDR P.Val
ACOT7	3,03	3,14E-11	3,54E-07	PDZD2	-4,67	1,38E-08	1,60E-05
C6orf136	4,08	3,30E-11	3,54E-07	BIRC3	-6,24	1,40E-08	1,60E-05
SLC29A1	3,08	2,18E-10	1,56E-06	DENND4C	-2,27	1,49E-08	1,60E-05
ALG3	3,54	5,19E-10	2,78E-06	PLAU	-3,11	6,39E-08	4,45E-05
SRM	3,08	1,49E-09	6,37E-06	GADD45A	-2,71	6,42E-08	4,45E-05
CTPS1	2,51	1,93E-09	6,72E-06	PARP14	-2,99	8,71E-08	5,42E-05
MMACHC	2,6	2,19E-09	6,72E-06	MTUS1	-3,34	8,84E-08	5,42E-05
DPAGT1	2,33	3,64E-09	9,17E-06	KDM5B	-2,39	9,77E-08	5,77E-05
HMGA2	4,54	3,85E-09	9,17E-06	GBP4	-4,77	1,33E-07	7,48E-05
ETV4	3,32	4,90E-09	1,05E-05	INPP1	-2,78	3,09E-07	0,0001

UTSCC-24A Collagen							
UP				DOWN			
Gene	Fold change	P.Val	FDR P.Val	Gene	Fold change	P.Val	FDR P.Val
SCNN1G	4,75	9,31E-06	0,0399	INPP5D	-2,09	4,69E-06	0,0305
GATSL3	2,25	2,95E-05	0,0752	DRD1	-2,08	0,0004	0,1709
CLEC7A	2,31	3,74E-05	0,0802	DNAH5	-4,81	0,0004	0,1711
ZNF358	2,24	7,25E-05	0,1197	SAMD4A	-2,07	0,0008	0,2306
MAFB	2,15	0,0001	0,1285	ZNF254	-2,05	0,0008	0,2330
ZNF114	2,29	0,0001	0,1432	ZNF257	-2,04	0,0015	0,2620
HCFC1R1	2,25	0,0002	0,1432	TMEM2	-2,54	0,0020	0,2887
SMAD6	2,85	0,0002	0,1432	EPB41	-2,11	0,0031	0,3212
SLC29A2	2,29	0,0002	0,1433	SACS	-2,01	0,0063	0,3651
GRAMD1A	2,04	0,0003	0,1490	FAP	-2,42	0,0080	0,3792

UTSCC-24B BSA							
UP				DOWN			
Gene	Fold change	P.Val	FDR P.Val	Gene	Fold change	P.Val	FDR P.Val
RP11-93O14.2; VPS35	3,07	0,0002	0,7258	PLCB4	-2,47	0,0002	0,7258
B4GALNT2	2,08	0,0015	0,9776	IL16	-2,32	0,0020	0,9776
GSTM5	2,42	0,0018	0,9776	ATXN7L3	-2,2	0,0049	0,9776
CNR2	2,46	0,0022	0,9776	PTPN13	-2,01	0,0275	0,9998
FMO1	2,11	0,0027	0,9776	RASGEF1B	-2,02	0,0279	0,9998
CYP39A1	2,02	0,0038	0,9776	KDM4C	-2,03	0,0459	0,9998
ACKR3	2,36	0,0054	0,9776				
THEM6	2,09	0,0062	0,9865				
RPS3A	2,95	0,0081	0,9998				
OR4F21	2,11	0,0126	0,9998				

UTSCC-24B Matrigel							
UP				DOWN			
Gene	Fold change	P.Val	FDR P.Val	Gene	Fold change	P.Val	FDR P.Val
GSTM5	3,71	5,30E-05	0,6723	LGALS4	-2,33	0,0010	0,6723
HBEGF	2,16	0,0010	0,6723	HNRNPA1P33; LINC00842; ANXA8L1	-2,27	0,0017	0,6723
AMT; NICN1	2,07	0,0019	0,6723	ANO6	-2,02	0,0046	0,7042
DACT1	2,01	0,0030	0,7042	TMEM27	-2,61	0,0088	0,7217
CXCL3	2,3	0,0036	0,7042	PTPN13	-2,07	0,0142	0,8013
ANGPTL8	2,15	0,0061	0,7163	PLCB4	-2,05	0,0143	0,8013
CCL20	2,26	0,0063	0,7163	RASGEF1B	-2,05	0,0230	0,8569
EDNRA	2,27	0,0073	0,7217	MFAP5	-2,05	0,0393	0,8989
GSTM1	2,72	0,0078	0,7217				
RUFY1	2,09	0,0097	0,7335				

UTSCC-24B Fibronectin							
UP				DOWN			
Gene	Fold change	P.Val	FDR P.Val	Gene	Fold change	P.Val	FDR P.Val
GSTM5	2,53	0,0006	0,9095	IL16	-2,21	0,0021	0,9992
CHRNB1	2,02	0,0012	0,9095	AMN1	-2,01	0,0044	0,9992
THNSL2	2,07	0,0025	0,9992	PPM1B	-2,26	0,0343	0,9992
MAP3K12	2,26	0,0046	0,9992				
MYL9	2,28	0,0060	0,9992				
CNIH2	2,07	0,0063	0,9992				
GGT5	2,01	0,0092	0,9992				
RFX3	2,36	0,0146	0,9992				
CAPN5	2,02	0,0165	0,9992				
TRPV4	2,26	0,0216	0,9992				

UTSCC-24B Myogel							
UP				DOWN			
Gene	Fold change	P.Val	FDR P.Val	Gene	Fold change	P.Val	FDR P.Val
SERPINE1	2,62	7,67E-06	0,1645	IL16	-2,37	0,0075	0,9008
MYL9	3,41	0,0008	0,8757	AADAC	-2,19	0,0190	0,9858
OLFM1	2	0,0010	0,8757	MAGEE1	-2,02	0,0239	0,9991
SPOCK1	2,03	0,0017	0,8757				
GSTM5	2,29	0,0026	0,8761				
FMO1	2,37	0,0038	0,9001				
TAGLN	2,4	0,0160	0,9777				
VIM	2,18	0,0306	0,9991				
RPS3A	2,1	0,0356	0,9991				

UTSCC-24B Fibrin							
UP				DOWN			
Gene	Fold change	P.Val	FDR P.Val	Gene	Fold change	P.Val	FDR P.Val
MMP10	3,16	7,33E-07	0,0157	DHRS3; MIR6730	-2,37	5,09E-05	0,0570
LY6K	2,38	2,30E-06	0,0247	GPSM2	-2,22	0,0001	0,0761
NHLRC1	2,36	4,66E-06	0,0251	CCNB2	-2,31	0,0002	0,0777
LCE3D	4,07	7,11E-06	0,0260	CCNB1	-2,04	0,0002	0,0777
LAMA3	2,5	1,08E-05	0,0260	TMEM52B	-2,44	0,0003	0,0842
MAPK8IP3	2,87	1,09E-05	0,0260	PTTG2	-2,01	0,0005	0,0996
TGFB1I1	2,16	2,45E-05	0,0359	OLR1	-2,63	0,0011	0,1530
RPS3A	4,36	3,52E-05	0,0444	LGALS4	-2,22	0,0017	0,1756
ZBED2	2,34	7,32E-05	0,0661	BBS4	-2,02	0,0025	0,1992
SERTAD1	2,14	7,40E-05	0,0661	BIRC3	-2,18	0,0034	0,2095

UTSCC-24B Collagen							
UP				DOWN			
Gene	Fold change	P.Val	FDR P.Val	Gene	Fold change	P.Val	FDR P.Val
CSF1	2,07	3,08E-05	0,0825	SPRR1B	-4,89	0,0003	0,2687
KRTAP2-2	2,63	0,0001	0,1733	KLK10	-5,66	0,0005	0,3490
ATF3	2,1	0,0002	0,2146	PLCB4	-2,4	0,0005	0,3803
GPRC5B	2,25	0,0002	0,2146	IL16	-2,39	0,0010	0,4299
MAP3K12	2,25	0,0004	0,3281	SLFN5	-2,4	0,0010	0,4299
CNIH2	2,43	0,0004	0,3281	SPRR1A	-6,41	0,0015	0,4311
GRAMD1A	2,13	0,0006	0,3867	A2ML1	-3	0,0030	0,4311
ARHGAP33	2,07	0,0013	0,4311	SPRR3	-8,06	0,0032	0,4311
MICAL2	2,33	0,0017	0,4311	SPRR2B	-2,86	0,0041	0,4707
GSTM5	2,32	0,0027	0,4311	IL13RA2	-2,65	0,0057	0,4906

Supplementary table 4: **Number of differentially expressed pathways of UT-SCC 24A and B cultured on different matrices.** Results of the gene set enrichment analysis (GSEA) showing the number of the differentially represented pathways between cells cultured on plastic and cells cultured on matrices. The pathways that passed the filter criteria had a $p<0.05$.

Cell line /Matrix	Number of affected pathways	
	Up	Down
UTSCC-24A /BSA	23	30
UTSCC-24A /Matrigel	163	253
UTSCC-24A / Fibronectin	11	158
UTSCC-24A /Myogel	194	126
UTSCC-24A /Fibrin	204	347
UTSCC-24A /Collagen	7	10
UTSCC-24B /BSA	16	8
UTSCC-24B /Matrigel	53	9
UTSCC-24B /Fibronectin	48	3
UTSCC-24B /Myogel	26	23
UTSCC-24B /Fibrin	107	117
UTSCC-24B /Collagen	135	13

Supplementary table 5: The 10 most affected pathways of UT-SCC cells cultured on different matrices. Results of the gene set enrichment analysis (GSEA) showing the 10 most differentially expressed pathways between cells cultured on plastic and cells cultured on matrices. The pathways that passed the filter criteria had a $p<0.05$.

UTSCC-24-A BSA					
Down			**Up**		
Pathway	**P.Val**	**q.Val**	**Pathway**	**P.Val**	**q.Val**
GO:0019722 calcium-mediated signaling	0,010398	0,798518	GO:0055114 oxidation-reduction process	0,000219	0,276044
GO:0043279 response to alkaloid	0,015946	0,798518	GO:0022900 electron transport chain	0,003323	0,959301
GO:0006816 calcium ion transport	0,018369	0,798518	GO:0022904 respiratory electron transport chain	0,00629	0,959301
GO:0070838 divalent metal ion transport	0,018369	0,798518	GO:0015980 energy derivation by oxidation of organic compounds	0,008081	0,959301
GO:0072511 divalent inorganic cation transport	0,018369	0,798518	GO:0006091 generation of precursor metabolites and energy	0,008506	0,959301
GO:0006260 DNA replication	0,018722	0,798518	GO:0045333 cellular respiration	0,008795	0,959301
GO:0043269 regulation of ion transport	0,018837	0,798518	GO:0072594 establishment of protein localization to organelle	0,011028	0,959301
GO:0055001 muscle cell development	0,021188	0,798518	GO:0070585 protein localization to mitochondrion	0,012692	0,959301
GO:0000226 microtubule cytoskeleton organization	0,023072	0,798518	GO:0072655 establishment of protein localization to mitochondrion	0,012692	0,959301
GO:0015749 monosaccharide transport	0,025319	0,798518	GO:0002495 antigen processing and presentation of peptide antigen via MHC class II	0,015399	0,959301

UTSCC-24-A Matrigel					
Down			**Up**		
Pathway	**P.Val**	**q.Val**	**Pathway**	**P.Val**	**q.Val**
GO:0007010 cytoskeleton organization	6,37E-08	0,000134	GO:0006396 RNA processing	9,83E-14	2,06E-10
GO:0030029 actin filament-based process	1,41E-06	0,00148	GO:0034660 ncRNA metabolic process	3,91E-12	4,11E-09
GO:0007155 cell adhesion	1,09E-05	0,005751	GO:0034470 ncRNA processing	4,29E-11	3,01E-08
GO:0022610 biological adhesion	1,09E-05	0,005751	GO:0022613 ribonucleoprotein complex biogenesis	6,39E-11	3,35E-08
GO:0030036 actin cytoskeleton organization	2,3E-05	0,009685	GO:0042254 ribosome biogenesis	7,55E-10	3,17E-07
GO:0034330 cell junction organization	5,59E-05	0,019562	GO:0016071 mRNA metabolic process	1,47E-07	5,16E-05
GO:0031589 cell-substrate adhesion	7,34E-05	0,022017	GO:0006364 rRNA processing	3,24E-07	9,73E-05
GO:0032970 regulation of actin filament-based process	0,000124	0,030913	GO:0016072 rRNA metabolic process	7,53E-07	0,000198
GO:0007160 cell-matrix adhesion	0,000145	0,030913	GO:0006397 mRNA processing	4,07E-06	0,00095
GO:0045216 cell-cell junction organization	0,000147	0,030913	GO:0051320 S phase	5,92E-06	0,001244

UTSCC-24-A Fibronectin					
Down			**Up**		
Pathway	**P.Val**	**q.Val**	**Pathway**	**P.Val**	**q.Val**
GO:0034645 cellular macromolecule biosynthetic process	0,001043	0,29148	GO:0042742 defense response to bacterium	0,014335	0,998957
GO:0009059 macromolecule biosynthetic process	0,001436	0,29148	GO:0009581 detection of external stimulus	0,015075	0,998957
GO:0019219 regulation of nucleobase-containing compound metabolic process	0,001467	0,29148	GO:0055088 lipid homeostasis	0,018503	0,998957
GO:0051171 regulation of nitrogen compound metabolic process	0,002046	0,29148	GO:0009582 detection of abiotic stimulus	0,020825	0,998957
GO:0006184 GTP catabolic process	0,002151	0,29148	GO:0051606 detection of stimulus	0,025167	0,998957
GO:0046039 GTP metabolic process	0,002151	0,29148	GO:0006959 humoral immune response	0,030377	0,998957
GO:1901069 guanosine-containing compound catabolic process	0,002151	0,29148	GO:0050994 regulation of lipid catabolic process	0,032853	0,998957
GO:0007010 cytoskeleton organization	0,002357	0,29148	GO:0050727 regulation of inflammatory response	0,041464	0,998957
GO:0051056 regulation of small GTPase mediated signal transduction	0,003212	0,29148	GO:0007601 visual perception	0,044468	0,998957
GO:1901068 guanosine-containing compound metabolic process	0,003603	0,29148	GO:0050953 sensory perception of light stimulus	0,044468	0,998957

UTSCC-24-A Fibrin					
Down			**Up**		
Pathway	**P.Val**	**q.Val**	**Pathway**	**P.Val**	**q.Val**
GO:0006952 defense response	6,67E-07	0,000877	GO:0006396 RNA processing	1,69E-16	4,16E-13
GO:0006955 immune response	7,38E-07	0,000877	GO:0006259 DNA metabolic process	1,04E-14	1,27E-11
GO:0007155 cell adhesion	1,43E-06	0,000877	GO:0034660 ncRNA metabolic process	1,58E-13	1,29E-10
GO:0022610 biological adhesion	1,43E-06	0,000877	GO:0022613 ribonucleoprotein complex biogenesis	7,85E-12	4,83E-09
GO:0045087 innate immune response	3,31E-05	0,015217	GO:0034470 ncRNA processing	1,21E-11	5,97E-09
GO:0034341 response to interferon-gamma	3,71E-05	0,015217	GO:0006260 DNA replication	5,55E-10	2,28E-07
GO:0007009 plasma membrane organization	7,49E-05	0,026319	GO:0042254 ribosome biogenesis	2,88E-09	1,01E-06
GO:0032879 regulation of localization	9,19E-05	0,028262	GO:0006281 DNA repair	3,6E-09	1,11E-06
GO:0034340 response to type I interferon	0,000107	0,029263	GO:0000375 RNA splicing, via transesterification reactions	8,34E-08	2,06E-05
GO:0060337 type I interferon-mediated signaling pathway	0,000145	0,032422	GO:0006974 response to DNA damage stimulus	9,1E-08	2,06E-05

UTSCC-24-A Collagen					
Down			**Up**		
Pathway	**P.Val**	**q.Val**	**Pathway**	**P.Val**	**q.Val**
GO:0022403 cell cycle phase	0,000245	0,233147	GO:0045333 cellular respiration	0,000234	0,391614
GO:0000279 M phase	0,000279	0,233147	GO:0006415 translational termination	0,001179	0,671588
GO:0022402 cell cycle process	0,000738	0,41105	GO:0022904 respiratory electron transport chain	0,001206	0,671588
GO:0007010 cytoskeleton organization	0,001541	0,53362	GO:0006119 oxidative phosphorylation	0,001697	0,708556
GO:0000280 nuclear division	0,001917	0,53362	GO:0055114 oxidation-reduction process	0,002147	0,717234
GO:0007067 mitosis	0,001917	0,53362	GO:0006414 translational elongation	0,002766	0,769996
GO:0000087 M phase of mitotic cell cycle	0,002709	0,646275	GO:0022900 electron transport chain	0,004526	0,786938
GO:0051301 cell division	0,003417	0,694951	GO:0042773 ATP synthesis coupled electron transport	0,005327	0,786938
GO:0000278 mitotic cell cycle	0,003753	0,694951	GO:0042775 mitochondrial ATP synthesis coupled electron transport	0,005327	0,786938
GO:0048285 organelle fission	0,004161	0,694951	GO:0006612 protein targeting to membrane	0,005438	0,786938

UTSCC-24-B BSA					
Down			**Up**		
Pathway	**P.Val**	**q.Val**	**Pathway**	**P.Val**	**q.Val**
GO:0097194 execution phase of apoptosis	0,011799	0,920918	GO:0051641 cellular localization	0,005651	0,813626
GO:0008380 RNA splicing	0,020719	0,920918	GO:0051649 establishment of localization in cell	0,010146	0,813626
GO:0010629 negative regulation of gene expression	0,025815	0,920918	GO:0007155 cell adhesion	0,011226	0,813626
GO:0006470 protein dephosphorylation	0,03431	0,920918	GO:0022610 biological adhesion	0,011226	0,813626
GO:0000122 negative regulation of transcription from RNA polymerase II promoter	0,038486	0,920918	GO:0046907 intracellular transport	0,022417	0,813626
GO:0006397 mRNA processing	0,040605	0,920918	GO:0048193 Golgi vesicle transport	0,024211	0,813626
GO:0042493 response to drug	0,041845	0,920918	GO:0006887 exocytosis	0,034407	0,813626
GO:0010038 response to metal ion	0,043682	0,920918	GO:0016197 endosomal transport	0,034503	0,813626
GO:0008284 positive regulation of cell proliferation	0,051191	0,920918	GO:0006810 transport	0,038726	0,813626
GO:0051607 defense response to virus	0,054508	0,920918	GO:0051234 establishment of localization	0,039812	0,813626

UTSCC-24-B Matrigel					
Down			**Up**		
Pathway	**P.Val**	**q.Val**	**Pathway**	**P.Val**	**q.Val**
GO:0003206 cardiac chamber morphogenesis	0,013578	0,982757	GO:0044106 cellular amine metabolic process	0,002348	0,84309
GO:0051301 cell division	0,018055	0,982757	GO:0006022 aminoglycan metabolic process	0,002928	0,84309
GO:0002027 regulation of heart rate	0,020331	0,982757	GO:0030203 glycosaminoglycan metabolic process	0,004087	0,84309
GO:0003231 cardiac ventricle development	0,023727	0,982757	GO:0030154 cell differentiation	0,007178	0,84309
GO:0055008 cardiac muscle tissue morphogenesis	0,023737	0,982757	GO:0048869 cellular developmental process	0,007846	0,84309
GO:0048644 muscle organ morphogenesis	0,024646	0,982757	GO:0048872 homeostasis of number of cells	0,009208	0,84309
GO:0060415 muscle tissue morphogenesis	0,024646	0,982757	GO:0006026 aminoglycan catabolic process	0,009768	0,84309
GO:0003205 cardiac chamber development	0,027024	0,982757	GO:0006027 glycosaminoglycan catabolic process	0,009768	0,84309
GO:0000279 M phase	0,027491	0,982757	GO:1901615 organic hydroxy compound metabolic process	0,010316	0,84309
GO:0008643 carbohydrate transport	0,050101	0,982757	GO:0051707 response to other organism	0,011081	0,84309

UTSCC-24-B Fibronectin					
Down			**Up**		
Pathway	**P.Val**	**q.Val**	**Pathway**	**P.Val**	**q.Val**
GO:0006396 RNA processing	0,023569	0,99072	GO:0045664 regulation of neuron differentiation	0,000196	0,211548
GO:0007605 sensory perception of sound	0,039439	0,99072	GO:0010975 regulation of neuron projection development	0,000917	0,495676
GO:0006412 translation	0,042584	0,99072	GO:0050767 regulation of neurogenesis	0,00227	0,719754
GO:0034660 ncRNA metabolic process	0,051719	0,99072	GO:0051094 positive regulation of developmental process	0,004548	0,719754
GO:0007568 aging	0,054225	0,99072	GO:0030334 regulation of cell migration	0,006712	0,719754
GO:0007584 response to nutrient	0,07565	0,99072	GO:0051960 regulation of nervous system development	0,007756	0,719754
GO:0016071 mRNA metabolic process	0,081613	0,99072	GO:0060284 regulation of cell development	0,008452	0,719754
GO:0006260 DNA replication	0,095581	0,99072	GO:0006631 fatty acid metabolic process	0,009114	0,719754
GO:0006650 glycerophospholipid metabolic process	0,09733	0,99072	GO:0006633 fatty acid biosynthetic process	0,010337	0,719754
GO:0050954 sensory perception of mechanical stimulus	0,104833	0,99072	GO:2000026 regulation of multicellular organismal development	0,01046	0,719754

UTSCC-24-B Myogel					
Down			**Up**		
Pathway	**P.Val**	**q.Val**	**Pathway**	**P.Val**	**q.Val**
GO:0007606 sensory perception of chemical stimulus	0,008066	0,892335	GO:0022900 electron transport chain	0,003885	0,928695
GO:0008286 insulin receptor signaling pathway	0,008587	0,892335	GO:0007179 transforming growth factor beta receptor signaling pathway	0,004013	0,928695
GO:0044344 cellular response to fibroblast growth factor stimulus	0,011402	0,892335	GO:0007162 negative regulation of cell adhesion	0,007188	0,928695
GO:0071774 response to fibroblast growth factor stimulus	0,011402	0,892335	GO:0017015 regulation of transforming growth factor beta receptor signaling pathway	0,00806	0,928695
GO:0008543 fibroblast growth factor receptor signaling pathway	0,012062	0,892335	GO:0071559 response to transforming growth factor beta stimulus	0,009457	0,928695
GO:0032870 cellular response to hormone stimulus	0,012591	0,892335	GO:0071560 cellular response to transforming growth factor beta stimulus	0,009457	0,928695
GO:0032869 cellular response to insulin stimulus	0,01477	0,892335	GO:0007005 mitochondrion organization	0,013131	0,928695
GO:0071375 cellular response to peptide hormone stimulus	0,017589	0,892335	GO:0034470 ncRNA processing	0,021716	0,928695
GO:1901653 cellular response to peptide	0,017589	0,892335	GO:0090101 negative regulation of transmembrane receptor protein serine/threonine kinase signaling pathway	0,026867	0,928695
GO:0015711 organic anion transport	0,023199	0,892335	GO:0045664 regulation of neuron differentiation	0,028825	0,928695

UTSCC-24-B Fibrin					
Down			**Up**		
Pathway	**P.Val**	**q.Val**	**Pathway**	**P.Val**	**q.Val**
GO:0000087 M phase of mitotic cell cycle	0,000182	0,082771	GO:0009966 regulation of signal transduction	0,000752	0,738781
GO:0048285 organelle fission	0,000185	0,082771	GO:0048583 regulation of response to stimulus	0,001333	0,738781
GO:0000279 M phase	0,000209	0,082771	GO:0010627 regulation of intracellular protein kinase cascade	0,004032	0,738781
GO:0000280 nuclear division	0,000215	0,082771	GO:0023051 regulation of signaling	0,004094	0,738781
GO:0007067 mitosis	0,000215	0,082771	GO:0010646 regulation of cell communication	0,004923	0,738781
GO:0051301 cell division	0,000893	0,285167	GO:0009653 anatomical structure morphogenesis	0,006755	0,738781
GO:0007059 chromosome segregation	0,00131	0,285167	GO:0010720 positive regulation of cell development	0,007992	0,738781
GO:0043044 ATP-dependent chromatin remodeling	0,001404	0,285167	GO:0040011 locomotion	0,009103	0,738781
GO:0022403 cell cycle phase	0,001434	0,285167	GO:0048812 neuron projection morphogenesis	0,009379	0,738781
GO:0000278 mitotic cell cycle	0,001651	0,285167	GO:0007243 intracellular protein kinase cascade	0,009697	0,738781

UTSCC-24-B Collagen					
Down			**Up**		
Pathway	**P.Val**	**q.Val**	**Pathway**	**P.Val**	**q.Val**
GO:0030216 keratinocyte differentiation	9,39E-05	0,141949	GO:0001701 in utero embryonic development	0,001569	0,515809
GO:0009913 epidermal cell differentiation	0,00032	0,223352	GO:0009792 embryo development ending in birth or egg hatching	0,002963	0,515809
GO:0031424 keratinization	0,000443	0,223352	GO:0007548 sex differentiation	0,003068	0,515809
GO:0008544 epidermis development	0,002474	0,934403	GO:0008406 gonad development	0,003736	0,515809
GO:0034754 cellular hormone metabolic process	0,017461	0,997698	GO:0043009 chordate embryonic development	0,003974	0,515809
GO:0030855 epithelial cell differentiation	0,017953	0,997698	GO:0001501 skeletal system development	0,005503	0,515809
GO:0042445 hormone metabolic process	0,019827	0,997698	GO:0045597 positive regulation of cell differentiation	0,005561	0,515809
GO:0051494 negative regulation of cytoskeleton organization	0,022166	0,997698	GO:0045595 regulation of cell differentiation	0,006277	0,515809
GO:0018958 phenol-containing compound metabolic process	0,034323	0,997698	GO:0009887 organ morphogenesis	0,006369	0,515809
GO:0007218 neuropeptide signaling pathway	0,039086	0,997698	GO:0000209 protein polyubiquitination	0,00653	0,515809

Highlights

1) No single matrix can be used for all cell culture assays.
2) Selecting an appropriate matrix increases the reliability of *in vitro* cell culture assays.
3) Human tumor-derived matrix induces human carcinoma cell invasion
4) A Single cancer cell line cannot represent the behaviour of any cancer type due to cell lines diversity, especially in term of molecular response to the extracellular matrix.

Authors´ contributions:

Wafa Wahbi: Conceptualization, Methodology, Validation , Formal analysis , Software, Investigation , Data Curation, Writing - Original Draft , Writing - Review & Editing , Visualization , Project administration.

Ahmed Al-Samadi: Conceptualization, Methodology, Validation, Formal analysis, Software, Investigation, Data Curation, Writing - Review & Editing, Visualization, Project administration, Supervision.

Tuula Salo: Conceptualization, Methodology, Supervision, Writing - Review & Editing.

Reidar Grenman: Conceptualization, Methodology, Writing - Review & Editing.

Erika Naakka: Conceptualization, Data Curation, Formal analysis, Writing - Review & Editing

Katja Tuomainen: Conceptualization, Data Curation, Formal analysis, Writing - Review & Editing.

Ilida Suleymanova: Software, Writing - Review & Editing.

Annamari Arpalahti: Data Curation, Writing - Review & Editing.

Ilkka Miinalainen: Data Curation, Writing - Review & Editing.

Juho Vaananen: Formal analysis, Writing - Review & Editing.

Outi Monni: Methodology, Writing - Review & Editing.

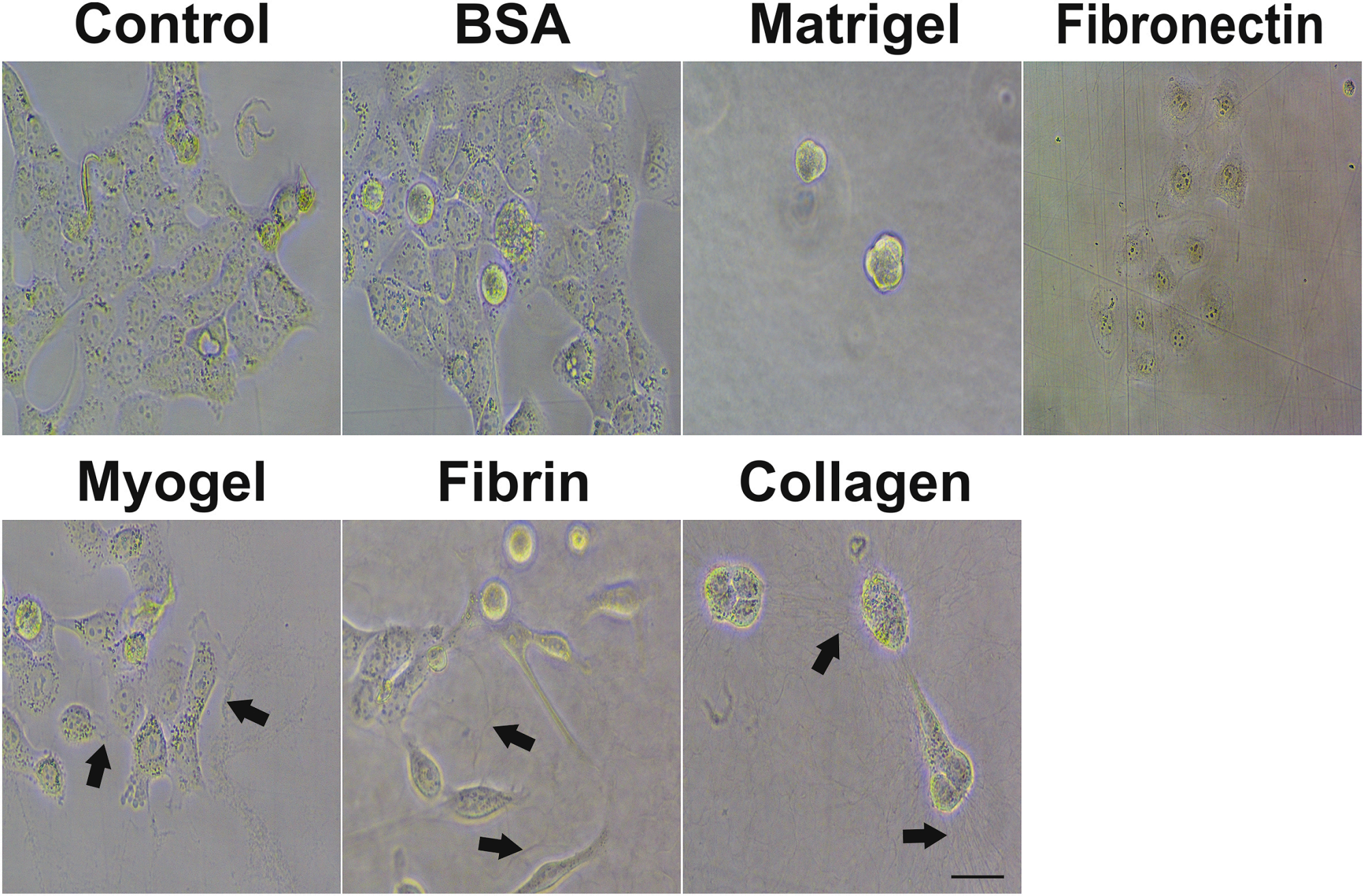
Control
BSA
Matrigel
Fibronectin
Myogel
Fibrin
Collagen

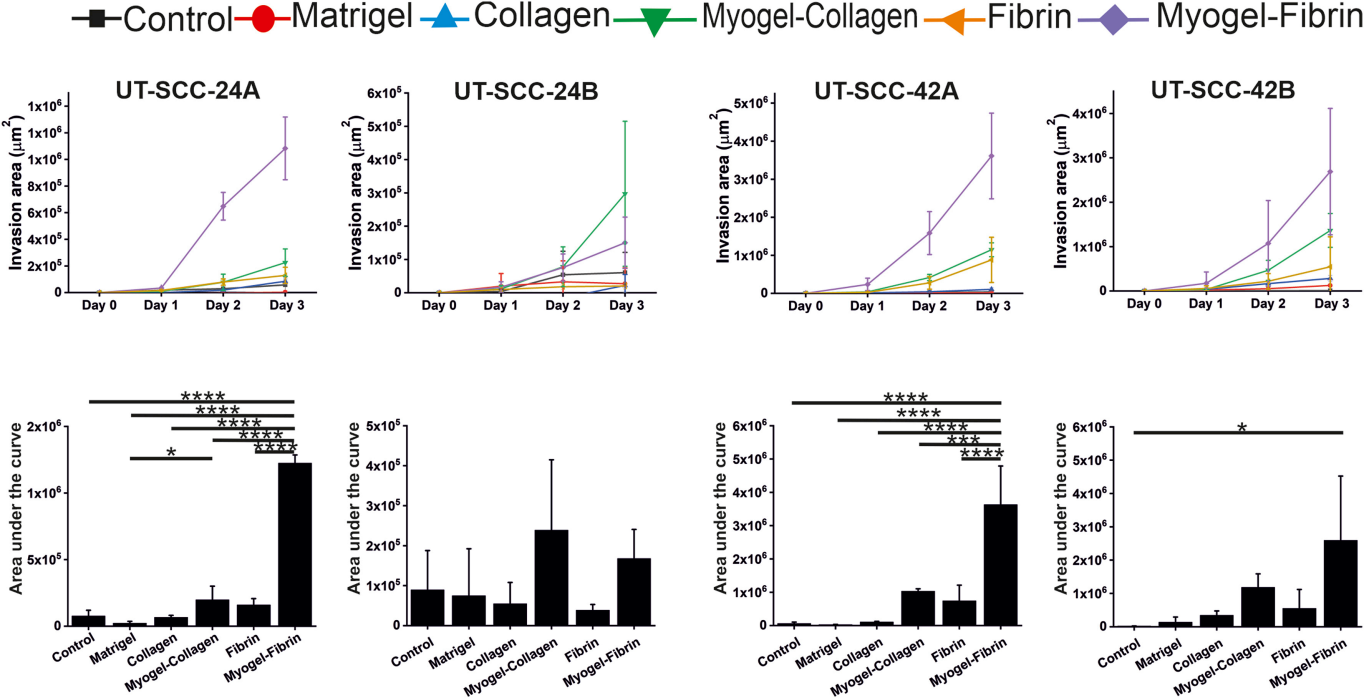
Control
Matrigel
Collagen
Myogel-Collagen
Fibrin
Myogel-Fibrin
UT-SCC-24A
UT-SCC-24B
UT-SCC-42A
UT-SCC-42B
Invasion area (μm²)
Day 0
Day 1
Day 2
Day 3
Area under the curve
Control
Matrigel
Collagen
Myogel-Collagen
Fibrin
Myogel-Fibrin
Myogel-Colagen
****
***
*

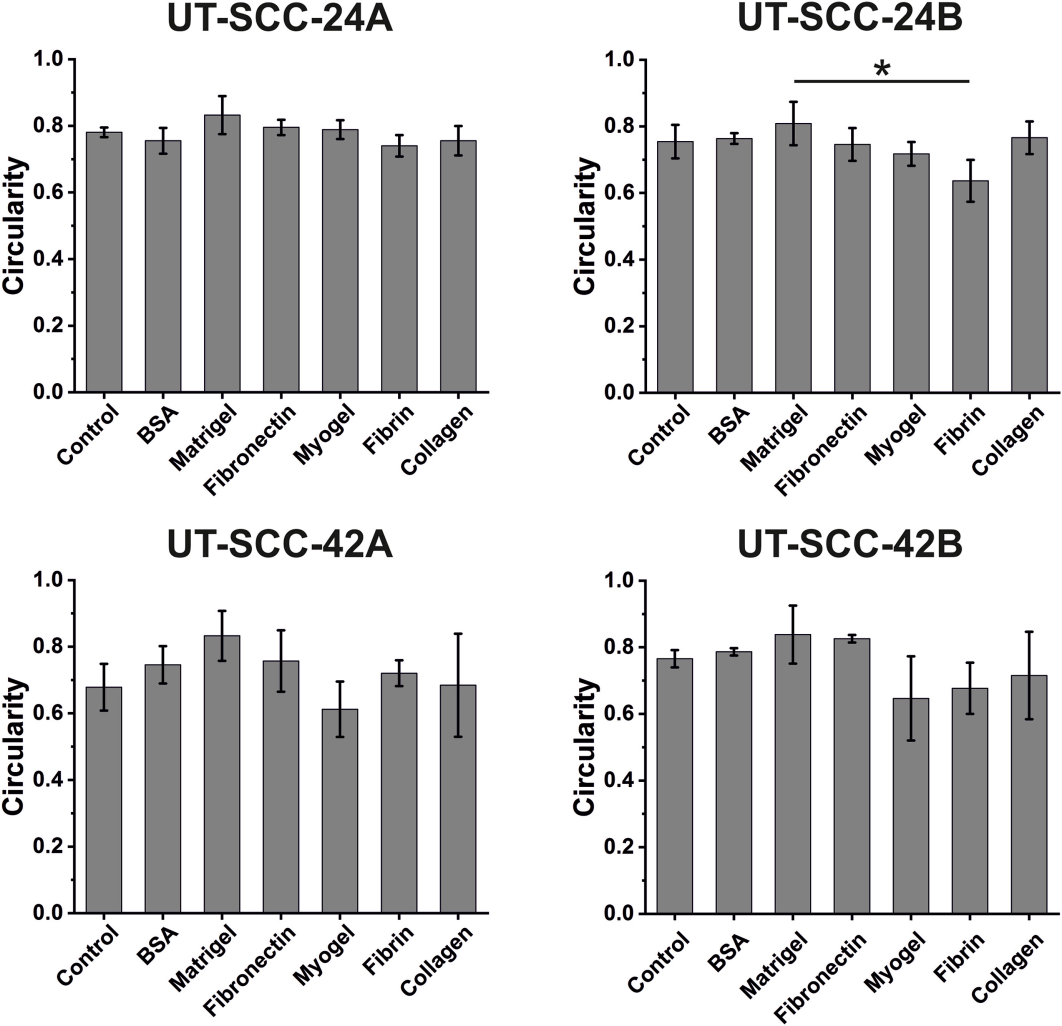
UT-SCC-24A
UT-SCC-24B
UT-SCC-42A
UT-SCC-42B
Circularity
1.0
0.8
0.6
0.4
0.2
0.0
*
Control
BSA
Matrigel
Fibronectin
Myogel
Fibrin
Collagen

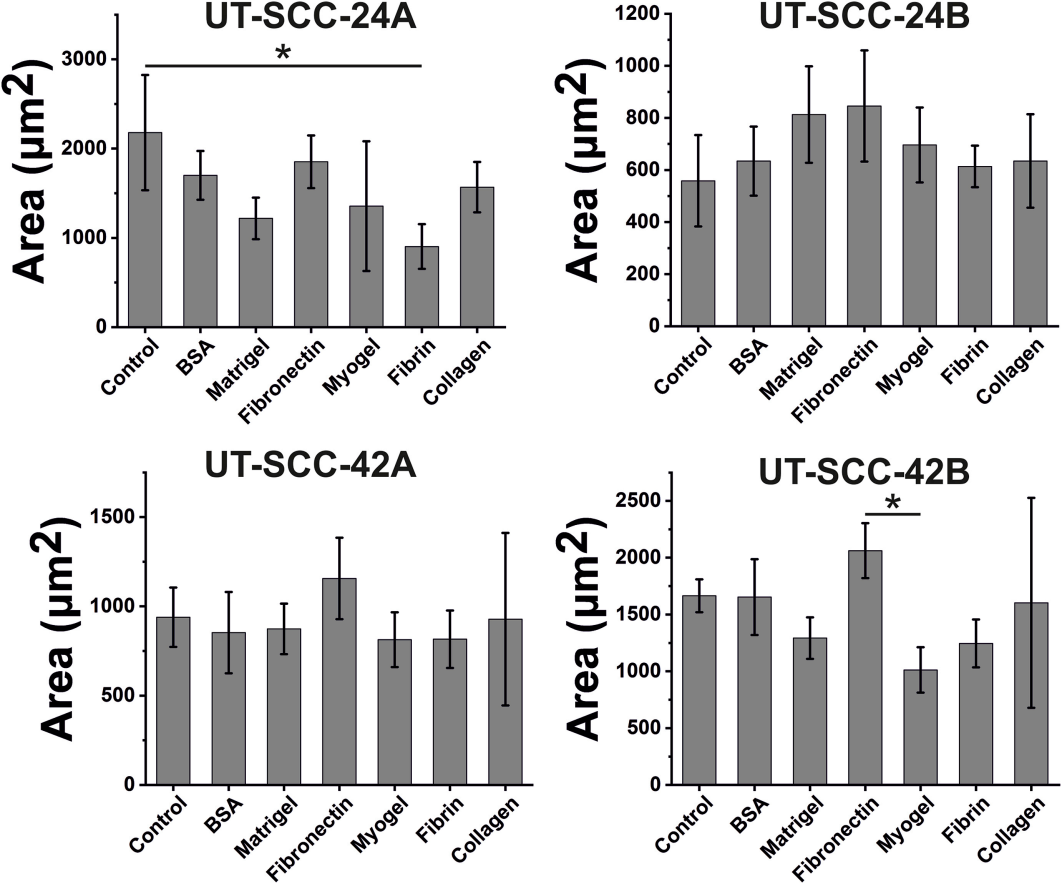
UT-SCC-24A
Area (μm2)
3000
2000
1000
0
*
Control
BSA
Matrigel
Fibronectin
Myogel
Fibrin
Collagen
UT-SCC-24B
Area (μm2)
1200
1000
800
600
400
200
0
Control
BSA
Matrigel
Fibronectin
Myogel
Fibrin
Collagen
UT-SCC-42A
Area (μm2)
1500
1000
500
0
Control
BSA
Matrigel
Fibronectin
Myogel
Fibrin
Collagen
UT-SCC-42B
Area (μm2)
2500
2000
1500
1000
500
0
*
Control
BSA
Matrigel
Fibronectin
Myogel
Fibrin
Collagen

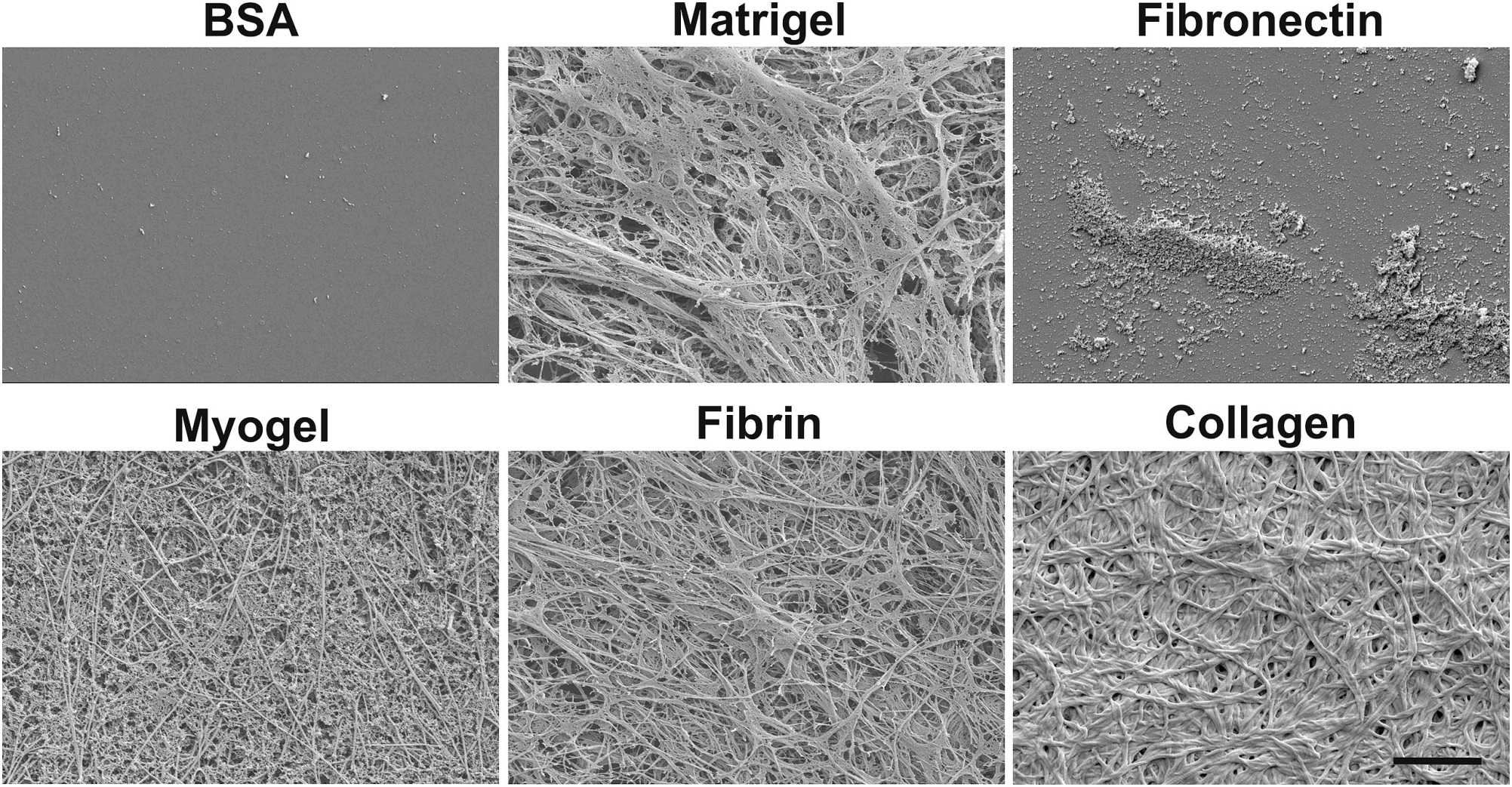
BSA
Matrigel
Fibronectin
Myogel
Fibrin
Collagen

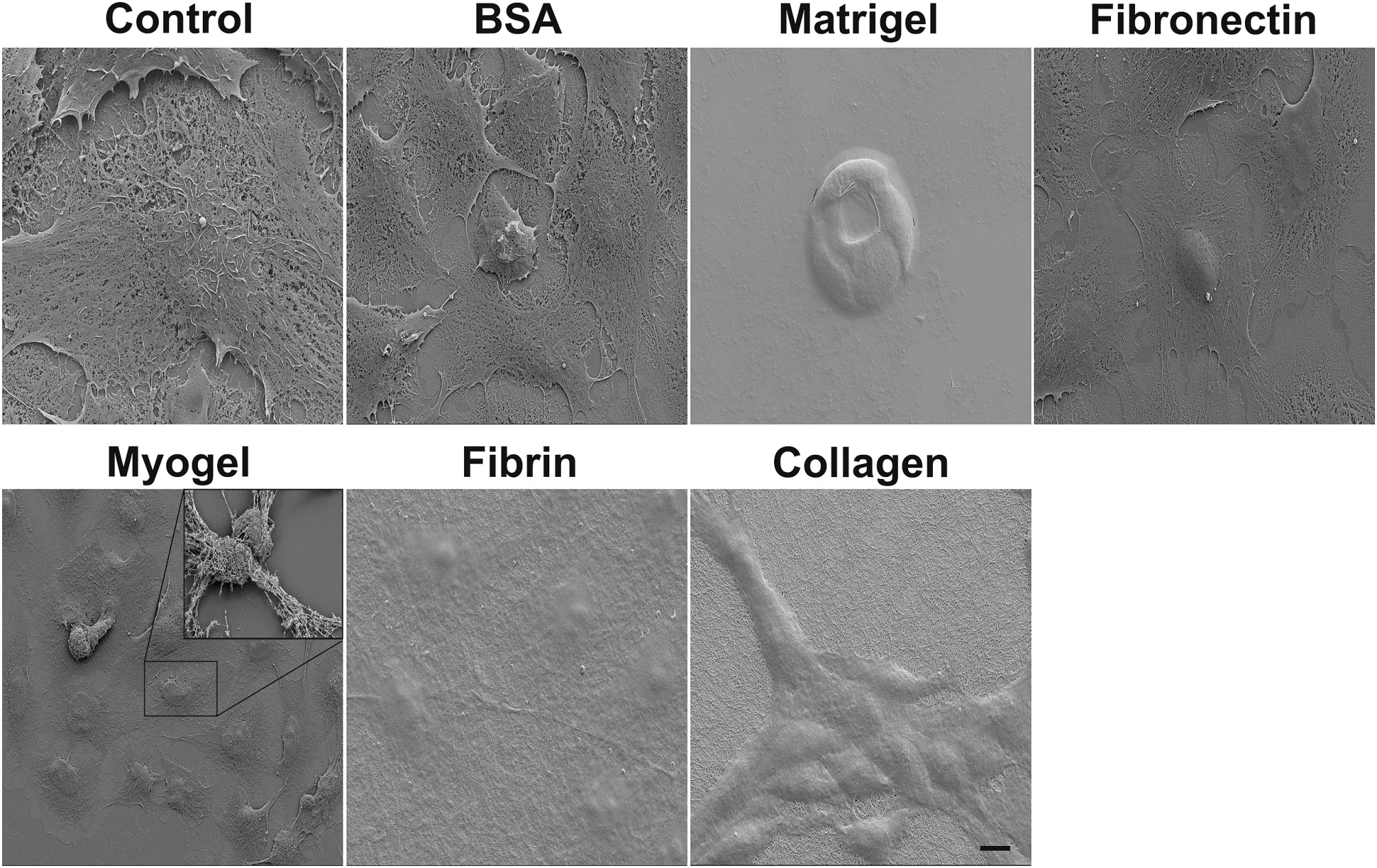
Control
BSA
Matrigel
Fibronectin
Myogel
Fibrin
Collagen

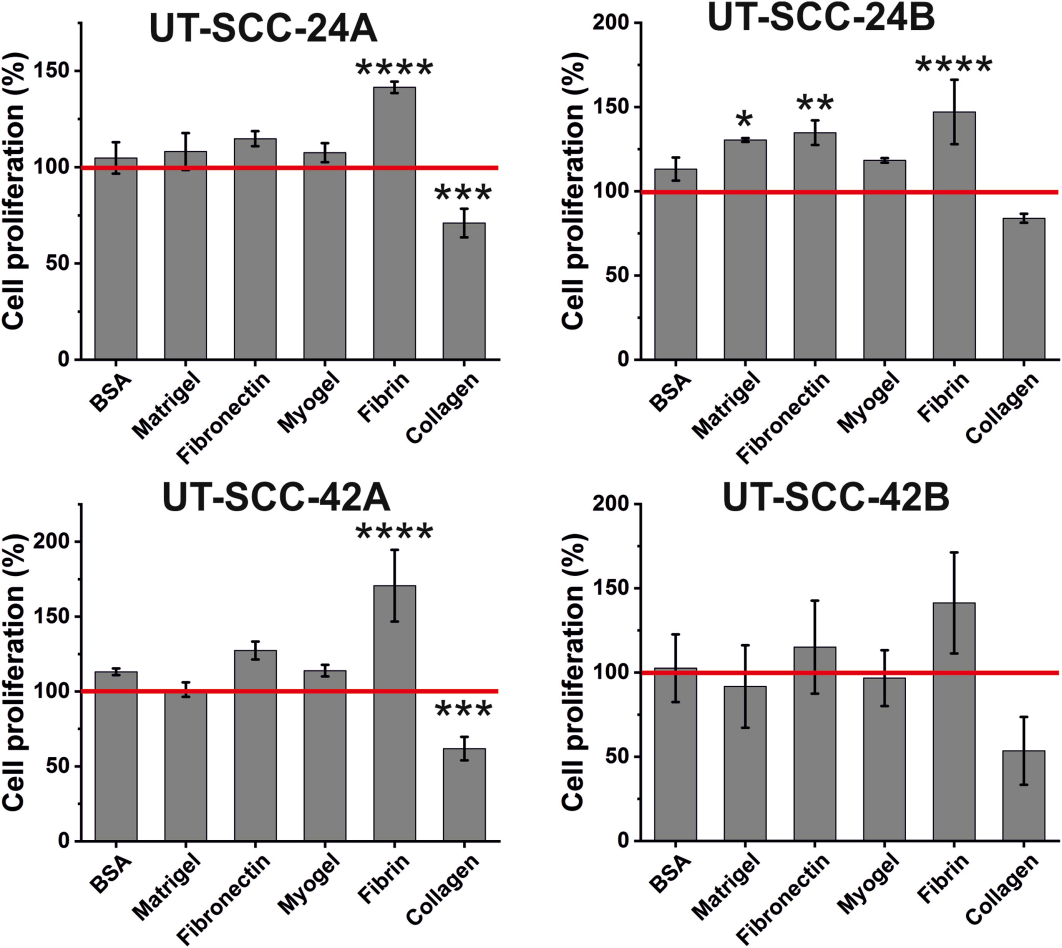
UT-SCC-24A
Cell proliferation (%)
150
100
50
0
****
***
BSA
Matrigel
Fibronectin
Myogel
Fibrin
Collagen
UT-SCC-24B
Cell proliferation (%)
200
150
100
50
0
*
**
****
BSA
Matrigel
Fibronectin
Myogel
Fibrin
Collagen
UT-SCC-42A
Cell proliferation (%)
200
150
100
50
0
****
***
BSA
Matrigel
Fibronectin
Myogel
Fibrin
Collagen
UT-SCC-42B
Cell proliferation (%)
200
150
100
50
0
BSA
Matrigel
Fibronectin
Myogel
Fibrin
Collagen

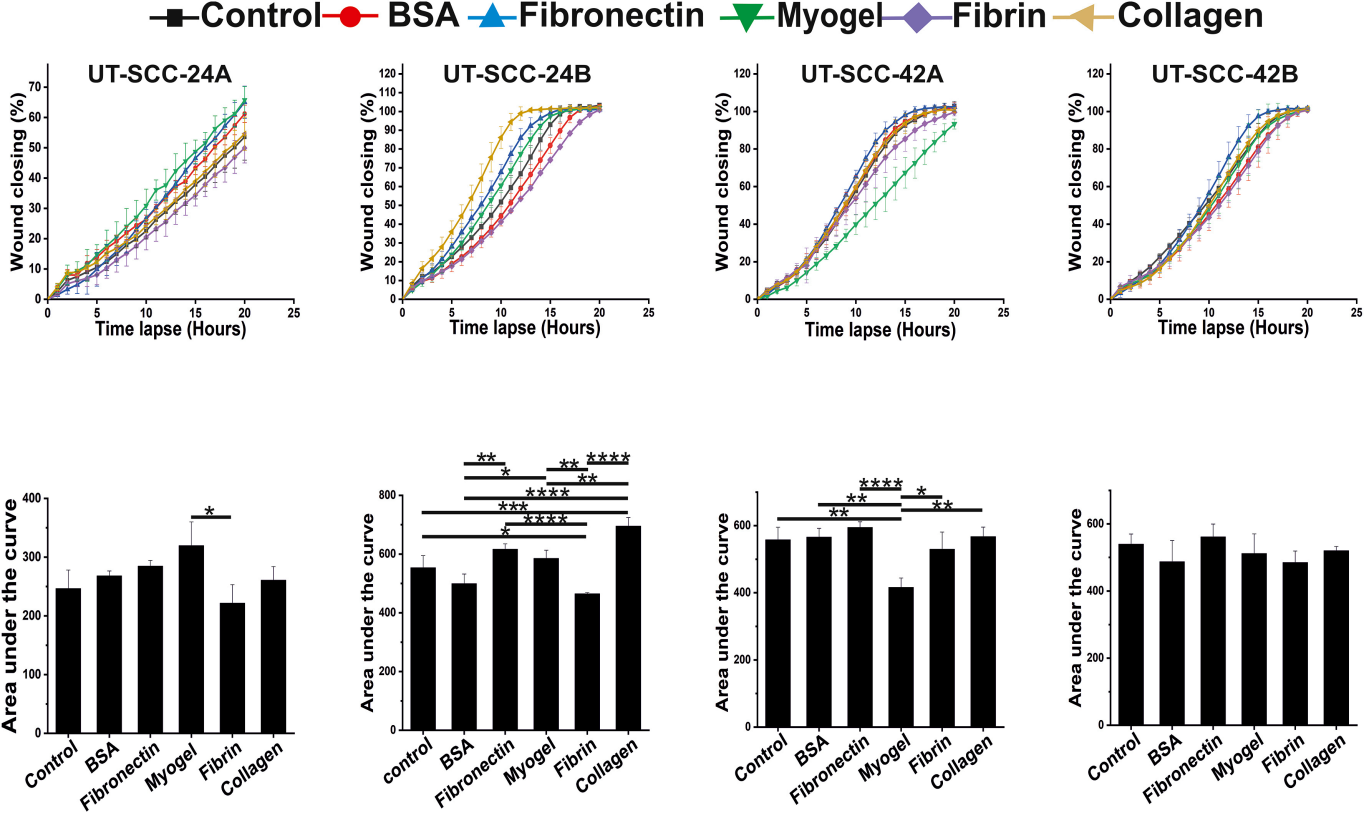
Control
BSA
Fibronectin
Myogel
Fibrin
Collagen
UT-SCC-24A
UT-SCC-24B
UT-SCC-42A
UT-SCC-42B
Wound closing (%)
Time lapse (Hours)
Area under the curve
Control
BSA
Fibronectin
Myogel
Fibrin
Collagen

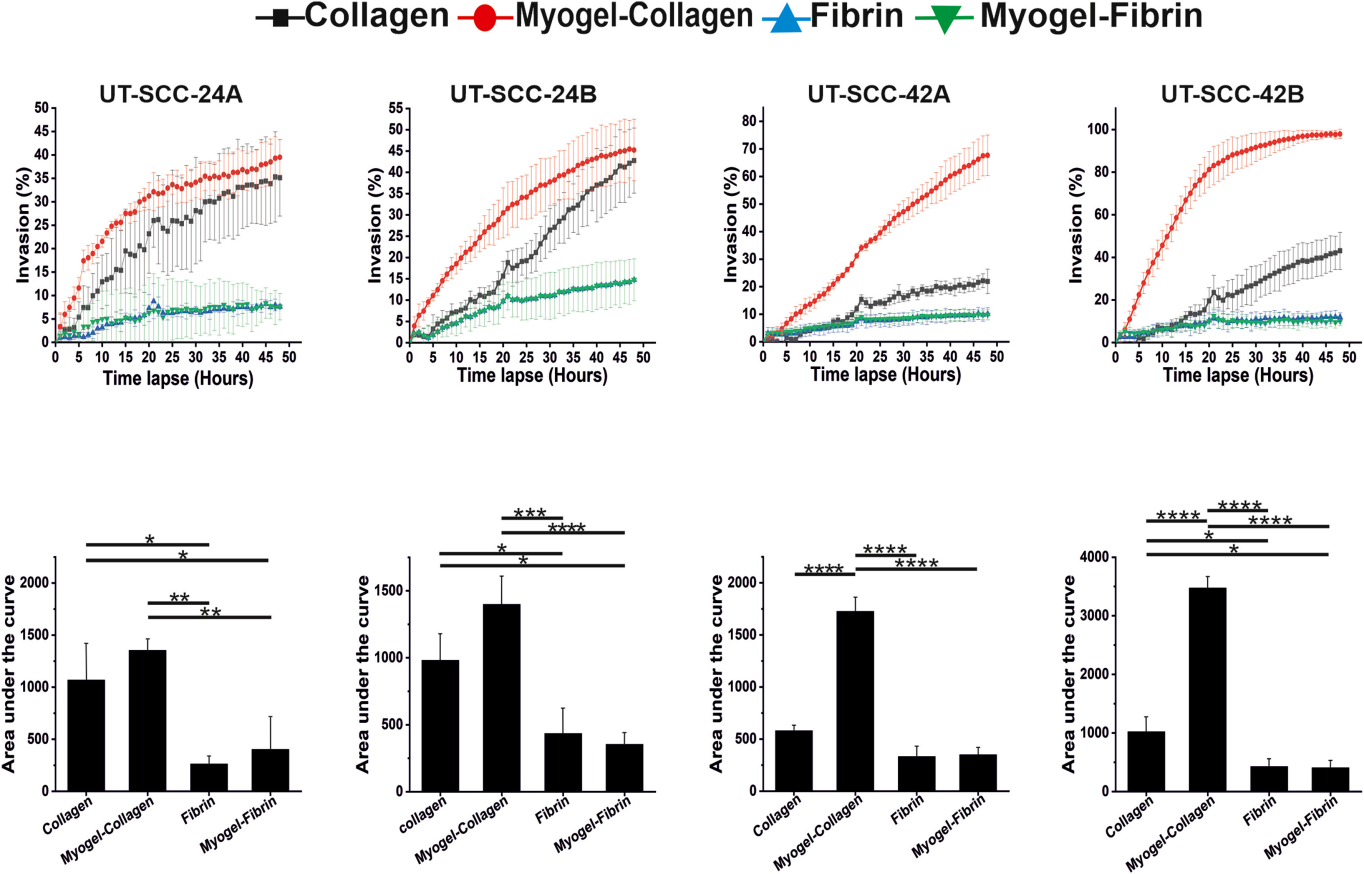
Collagen
Myogel-Collagen
Fibrin
Myogel-Fibrin
UT-SCC-24A
UT-SCC-24B
UT-SCC-42A
UT-SCC-42B
Invasion (%)
Time lapse (Hours)
Area under the curve
Collagen
Myogel-Collagen
Fibrin
Myogel-Fibrin

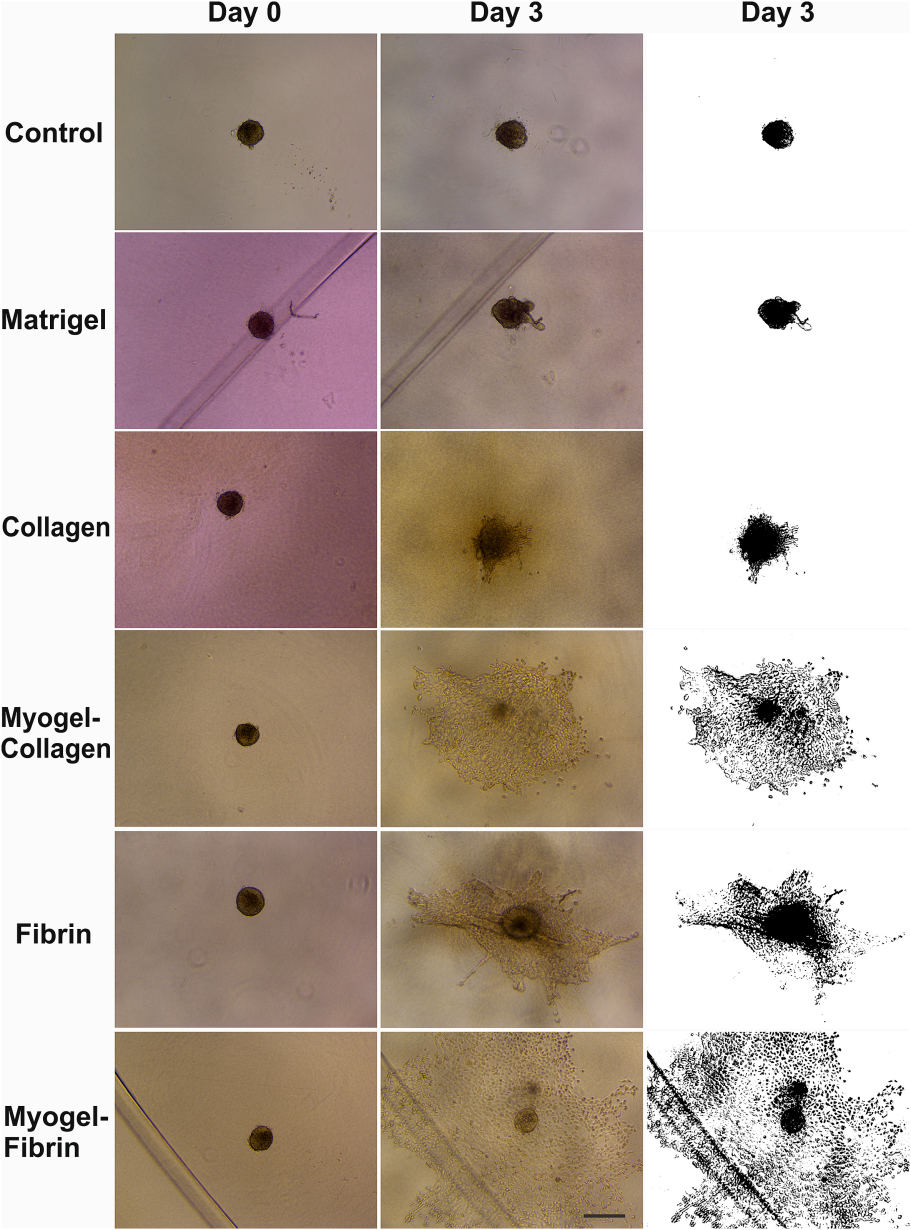
Day 0
Day 3
Day 3
Control
Matrigel
Collagen
Myogel-
Collagen
Fibrin
Myogel-
Fibrin

Declaration of interests

☒ The authors declare that they have no known competing financial interests or personal relationships that could have appeared to influence the work reported in this paper.

☐The authors declare the following financial interests/personal relationships which may be considered as potential competing interests: